AIChE

Kinetic Modeling of Catalytic Conversion of Methylcyclohexane over USY zeolites: Adsorption and Reaction Phenomena

Mustafa Al-Sabawi and Hugo de Lasa
Chemical Reactor Engineering Centre, Faculty of Engineering, University of Western Ontario, London, Ontario, Canada N6A 5B9

DOI 10.1002/aic.11825
Published online May 8, 2009 in Wiley InterScience (www.interscience.wiley.com).

Catalytic conversion of cycloparaffins is a complex process involving competing reaction steps. To understand this process, FCC experiments using methylcyclohexane (MCH) on USY zeolite catalysts were carried out in the mini-fluidized CREC riser simulator. Runs were developed under relevant FCC process conditions in terms of partial pressures of MCH, temperatures (450–550°C), contact times (3–7 s), catalyst-oil mass ratios (5), and using fluidized catalysts. MCH overall conversions ranged between 4 to 16 wt %, with slightly higher conversions obtained using the larger zeolite crystallites. Moreover, it was found that MCH undergoes ring opening, protolytic cracking, isomerization, hydrogen transfer and transalkylation. A heterogeneous kinetic model for MCH conversion including thermal effects, adsorption and intrinsic catalytic reaction phenomena was established. Adsorption and kinetic parameters were determined, including the heat of adsorption (−40 kJ/mol), as well as thermal and primary catalytic intrinsic activation energies, which were in the range of 43–69 kJ/mol, and 50–74 kJ/mol, respectively. © 2009 American Institute of Chemical Engineers *AIChE J,* 55: 1538–1558, 2009

Keywords: catalytic cracking, cycloparaffins, y zeolites, adsorption, kinetic modeling

Introduction

The volume of the upgrading of extra heavy oils and bitumens in Alberta, Canada to synthetic crude oils continues to rapidly expand. Continually improving economics, bolstered by high crude oil prices, has resulted in the international recognition of the vast potential of Canada's oil sands. However, the strong expansion of Canadian bitumen production brings many technical challenges that the industry needs to face. One of the concerns in Canadian bitumen-derived crude oil refining is the high content of heavy gas oil with a high percentage of both aromatics and cycloparaffins.

Aromatic fractions limit FCC bottoms conversion, decrease yield and quality of valuable products (gasoline and middle distillates), increase levels of polyaromatic hydrocarbons prone to form coke on the catalyst, and ultimately compromise the unit performance. Cycloparaffin (naphthene) conversion, on the other hand, is a complex process involving competing reaction steps such as cracking, hydrogen transfer, ring opening and isomerization. In this regard, cycloparaffins are important in cracking chemistry as precursors for aromatics.[1] It is through the detailed understanding of cycloparaffin catalytic cracking that one can influence the composition of the resulting gasoline, minimizing the total aromatics fraction and making it more environmentally friendly.

In spite of the significant effect that aromatics and cycloparaffins have on the processability of Canadian bitumen-derived crudes, there is limited information available in the open literature concerning the catalytic cracking of cycloparaffins over USHY zeolites under actual fluid catalytic cracking (FCC) conditions. Corma et al.[1] investigated the cracking

Correspondence concerning this article should be addressed to H. de Lasa at hdelasa@eng.uwo.ca

behavior of methylcyclohexane and methylcyclohexene over rare earth Y and USY zeolite catalysts using a microactivity fixed-bed glass tubular reactor at 500°C. These authors also carried out cracking experiments using decalin and tetralin over several zeolites using the same reactor.[2] Cerqueira et al.[3] studied the transformation of methylcyclohexane over HFAU, HMFI and HBEA zeolites with a range of famework Si/Al ratios at 450°C using a similar fixed-bed reactor. Mostad et al.[4] determined product distributions of decalin and tetralin over a USY-zeolite catalyst using a fixed-bed pulse reactor and a standard MAT-unit. Kubicka et al.[5,6] used an electrically heated 300-mL stainless-steel autoclave unit at 225–300°C to investigate the ring opening of decalin. It can be observed that all of the aforementioned cited experiments with cycloparaffins were conducted in standard microactivity test (MAT) units, small fixed beds that do not provide adequate simulation of large-scale FCC units in terms of reactant partial pressure, reaction contact time, temperature and catalyst/hydrocarbon ratios.

Modern commercial FCC catalyst particles consist of a matrix containing USY zeolite crystallites where most of the activity resides.[7] The matrix has large pores (macropores) that often exhibit some activity and behave as pre-cracking agents. These macropores also act as passageways for hydrocarbon molecules to diffuse from the surrounding environment into the particle interior, reaching the zeolite particles, which are considered to be the main component of commercial FCC catalysts. The USY zeolites provide the activity and selectivity of the catalysts. They consist of supercages that can inscribe 12.4 Å-dia. spheres. Rings composed of 12 oxygen atoms and having a free diameter of 7.4 Å act as openings into these supercages.[8] Each supercage cavity is connected to four other cavities, which are in turn connected to three-dimensional (3-D) cavities to form a highly porous structure.[9] It is within this pore structure that the locus of the adsorption capacity and catalytic activity reside for many reactions. Once reactant hydrocarbons reach a zeolite crystallite, they diffuse into its interior until they adsorb on the active sites on which they undergo chemical transformation. Since the pore sizes of the USY zeolite crystallites are generally of the same order of molecular dimension, molecules inside the micropores cannot escape the potential attraction of the zeolite pore walls. This means that molecules in the free form hardly exist, and mainly adsorbed molecules exist in the zeolite micropore.[10] It is, therefore, important to examine diffusion and adsorption phenomena in the zeolite pore network when catalytically cracking hydrocarbons.

Adsorption of hydrocarbons on the active sites of the zeolite crystallites is a necessary step for catalytic cracking reaction to occur.[11] The extent to which hydrocarbons are adsorbed depends significantly on reactor operating conditions, feedstock converted and catalyst properties. However, adsorption/desorption between the mobile phase and the adsorbed concentration on the framework often occurs rapidly compared to the time required for the overall transport, i.e. diffusion process, and consequently, adsorption takes place at close to equilibrium conditions.[12] Adsorption processes are critical in the modeling and simulation of continuous FCC riser units given that they strongly affect the volumetric flow of the gas phase and, consequently, the hydrocarbon contact time in the riser. Adsorption of hydrocarbon molecules on zeolites is well acknowledged, with heats of sorption ranging from 10 to 30 kcal/mol.[12] It is argued that heats of adsorption could be as high as 60 kcal/mol with adsorption of hydrocarbon molecules having, as a result, a significant effect on the overall energy balance of the FCC riser-regenerator unit.[12]

Besides, both diffusivity and adsorption of reactant guest molecules in zeolites are known to be highly dependent on treatment conditions such as dealumination or steaming.[13] Studies about the potential influence of such treatments on hydrocarbon adsorption are frequently limited to lower-temperatures (temperatures smaller than 350°C), and/or using less reactivity zeolites, which give data that is distant from relevant reaction conditions.[14,15,16,17] For instance, Denayer and Baron[18] investigated the effect of chain length and branching of paraffins in the gasoline range on adsorption and diffusion in various zeolites at 275–400°C. Atkinson and Curthoys[19] determined heats and entropies of adsorption of straight-chain, branched-chain and cyclic saturated hydrocarbons on cation-exchanged forms of zeolites X and Y at 300–500°C. Corma and Ortega[20] determined adsorption constants and heats of adsorption of n-hexadecane, 1-octene, decalin and tetralin on zeolitic catalysts at 400–500°C using a MAT-unit. Extrapolation of these data to actual FCC riser reaction temperatures in the 500–550°C is rather uncertain.

In addition, limited work has been developed to establish kinetic models for cycloparaffin catalytic cracking.[1,3] A major concern with these models is that they fail to consider the effects of hydrocarbon diffusion and adsorption in the catalyst pore network, but instead, they describe the combined effect of diffusion, adsorption and reaction using "pseudo-parameters". As a result, these models are of limited value for defining phenomenological based models account for the critical role of diffusion and adsorption in FCC.

To address these issues, this study considers catalytic cracking of cycloparaffins while carefully accounting for diffusion, adsorption and intrinsic kinetics. Experiments are developed using a cycloparaffin model compound, methylcyclohexane (MCH) and a USY zeolite in a CREC fluidized riser simulator.[21] a laboratory unit that has been extensively used in catalytic conversion and modeling studies.[22,23] This mini-fluidized bed overcomes the technical problems of the standard microactivity test (MAT), allowing catalytic cracking to be developed under relevant FCC conditions in terms of partial pressures of gas oil (1.5–2 atm), temperatures (450–550°C), contact times (3–7 s, both for the hydrocarbons and the catalyst), and catalyst-gas oil mass ratios (5). On this basis, diffusion, adsorption, intrinsic kinetic parameters are evaluated with the required statistical indicators. In this respect, this study represents a step forward toward an understanding of the role of chemical species adsorption and diffusion in zeolitic catalysts.

Experimentation

Reactant and catalysts

MCH (Alfa Aesar, 99% pure) catalytic cracking experiments were performed using two standard FCC catalysts. These two catalysts, which were characterized by Tonetto

Table 1. Properties* of the FCC Catalysts with Large and Small Crystallite Sizes

	Large Crystallite CAT-LC	Small Crystallite CAT-SC
Zeolite content (%)$^{+}$	29	31
Unit cell size (Å)	24.28	24.28
BET surface area (m^2/g)	197	169
External surface area (m^2/g)	20	25
Crystallite size (μm)	0.9	0.4
Crystallite density (kg/m^3)	825	825
Brønsted/Lewis Sites ratio @ 100°C	1	0.9

*Properties reported for USY zeolites after being pelletized and exchanged with ammonium nitrate.
$^{+}$Comparing area (BET) for zeolites, matrix and catalysts before steaming.

et al.[24] were prepared using the same procedure, and hence, have almost identical properties and characteristics (reported in Table 1), with the exception of the Y-zeolite crystallite size. One of the catalysts has 0.4 μm dia. crystallites (referred to as CAT-SC in this present study), and the other has larger 0.9 μm dia. crystallites (CAT-LC). Given that the only major difference between the two catalysts is the crystallite size, the quantitative evaluation of diffusional constraints could be carried out. The unit cell size was measured by X-ray diffraction following method ASTM D-3942-80, and the surface area was determined using the BET method.

Apparatus

Thermal and catalytic cracking experiments were performed in the Chemical Reactor Engineering Center (CREC) riser simulator using MCH. The CREC riser simulator is an experimental reactor, which operates isothermally and at constant volume of the reaction mixture. It enables injected MCH reactant to vaporize and, in the case of catalytic cracking reactions, come into contact and mix with fluidized catalyst throughout a predetermined time span. Well-mixed conditions are assumed to exist in the reactor as a result of the high gas recirculation rate, as reported by Ginsburg et al.[25] Further detailed information on the CREC riser simulator and its components can be found in Al-Sabawi et al.[26]

Pressure transducers are installed in both the reactor and the VB chambers to monitor the progress of each cracking experiment. A pressure profile in the CREC riser simulator for the catalytic cracking of MCH is shown in Figure 1. This figure shows that, before the injection of the feedstock into the reactor, the pressure of the reactor is 14.7 psia (1 atmosphere), whereas the VB is maintained at very low pressure (~1 psia). To maintain this difference in pressure, the reactor and VB are isolated by closing the four-port valve. At the time of injection of the MCH reactant into the reactor, the reactant rapidly vaporizes, causing an abrupt increase in pressure (A-B). Another stage follows the reactant vaporization whereby the gaseous MCH experiences cracking into different hydrocarbon products, causing an expansion in the system. As a result, a less pronounced pressure increase can be seen in the pressure profile (B-C). Once the preset reaction time is completed, the four-port valve is automatically switched to connect the reactor and the VB. The initial large difference in pressure between these two chambers causes the evacuation of the reaction products from the reactor into the VB. This evacuation, which occurs instantaneously due to the significant differences in pressure and volume between the reactor and VB, leads to a sudden drop in the reactor pressure and consequent rapid pressure stabilization in both chambers (C-D). Note that any further cracking of products present in the VB is abolished due to the low-temperature at which the VB is held (260°C).

Experimental conditions

Experiments involving the thermal and catalytic cracking of MCH were carried out at five temperatures of 450°C, 475°C, 500°C, 525 and 550°C and three reaction times of 3, 5, and 7 s. The catalytic cracking experiments were performed using a consistent catalyst/MCH ratio of 5 (weight of catalyst = 0.81 g, weight of injected MCH = 0.162 g).

Cracking Results

Thermal cracking results

MCH conversions were determined for each thermal cracking experiment and some of these conversions are reported in Figure 2. It is apparent that MCH conversion is significant under the selected reaction conditions of this study, especially at high-temperatures (550°C) and 7 s contact time, under which the overall conversion exceeds 4 wt %. What makes thermal cracking even more relevant is given by the fact that catalytic cracking experiments performed under similar reaction temperatures using a USY zeolite catalyst provided overall conversions of about 16 wt %. Hence, thermal cracking should not be neglected when examining the processability and the kinetic modeling of MCH, and cycloparaffins in general, during FCC operation.

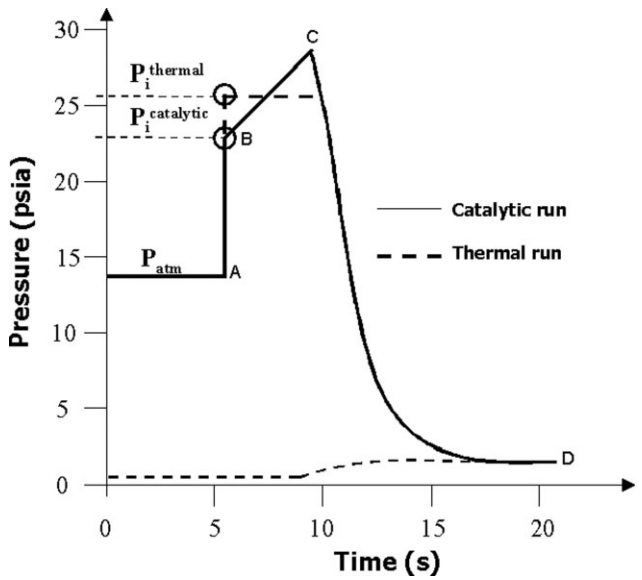

Figure 1. Typical pressure profile in the CREC riser simulator during MCH thermal and catalytic cracking runs.

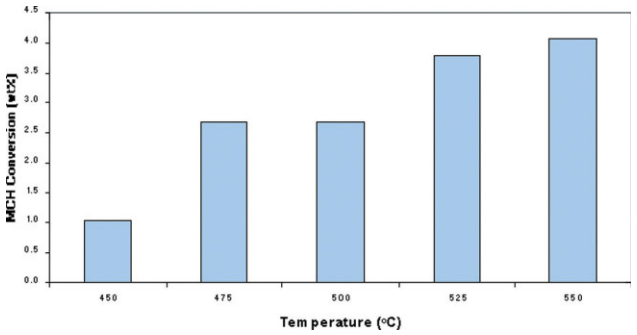

Figure 2. MCH conversion during thermal cracking in the CREC riser simulator at different temperatures and reaction time of 7 s.

[Color figure can be viewed in the online issue, which is available at www.interscience.wiley.com.]

Catalyst activity results – overall MCH conversion

An important objective of this study is to analyze MCH conversion at typical catalytic cracking conditions using both CAT-LC and CAT-SC catalysts. It is observed that the overall MCH conversion increases with both temperature and reaction time. Figures 3 and 4 illustrate this trend for CAT-LC and CAT-SC, respectively. For instance, for experiments conducted at 500°C using CAT-LC, the MCH conversions are 8.7, 10.9 and 13.0 wt % at reaction 3, 5 and 7 s, respectively. In this respect, the MCH conversion augments by 2 wt % when increasing the reaction time from 3 to 5 s, as well as from 5 to 7 s. Similar trends are observed using CAT-SC at the same reaction temperature, with the MCH conversions being 5.8, 8.8 and 11.3 wt % at reaction times of 3, 5 and 7 s, respectively. It is important to note that the MCH conversion values reported in Figures 3 and 4 are average values obtained using at least four repeat experiments at each of the reaction conditions proposed in this study. Maximum errors for the MCH conversion were 1.3 wt %.

It is observed that increasing the temperature for a given reaction time causes a steady increase in the overall MCH conversion. On this basis and on the parameter data fitting reported later in this study, it is possible to assume that the catalytic cracking reaction under the conditions of the CREC riser simulator displayed an apparent activation energy that did not change with temperature. Furthermore, while examining MCH conversions on USY catalysts, it can be noticed that the overall rate of conversion is not affected by pore diffusion resistance within the crystallite network. This would seem to be the case as the larger zeolite crystallites provide slightly higher MCH conversions than their smaller counterparts, as shown in Figure 5. In this figure, the conversion of MCH attained using CAT-LC is compared to the conversion obtained using CAT-SC. Experimental points that fall on or are close to the solid line show that CAT-LC and CAT-SC provide similar MCH conversions, whereas points that are farther away from the solid line denote differences in conversions between the two zeolite catalysts. It is apparent from this figure that, under all reaction conditions, CAT-LC yields mildly higher MCH conversions than CAT-SC. CAT-SC, with its smaller zeolite crystallites, would

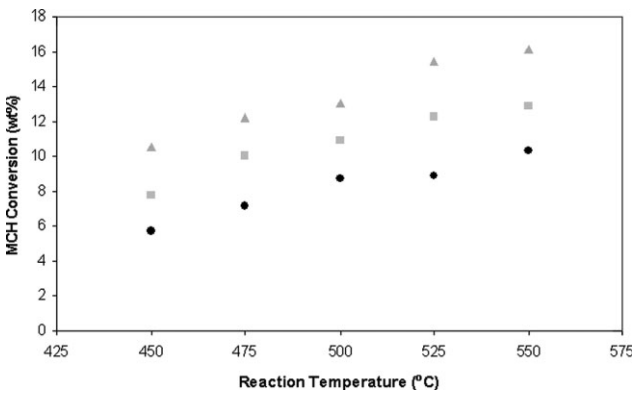

Figure 3. Conversion of MCH over CAT-LC at different temperatures.

Experiments were conducted at reaction times of 3 s (●), 5 s (■), and 7 s (▲) using a catalyst-gas oil ratio of 5.

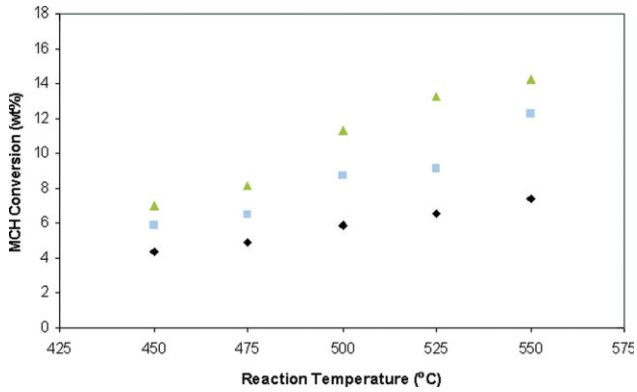

Figure 4. Conversion of MCH over CAT-SC at different temperatures.

Experiments were conducted at reaction times of 3 s (●), 5 s (■), and 7 s (▲) using a catalyst-gas oil ratio of 5. [Color figure can be viewed in the online issue, which is available at www.interscience.wiley.com.]

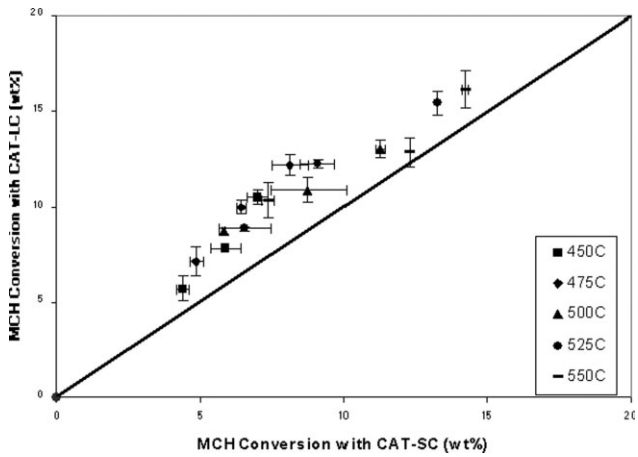

Figure 5. MCH conversion obtained using CAT-LC vs. CAT-SC.

Experiments were conducted using a catalyst-gas oil ratio of 5.

Table 2. Product Yields and Selectivities Obtained During MCH Catalytic Cracking Over CAT-LC and CAT-SC at 550°C and 7 s

Products	CAT-LC		CAT-SC	
	Yield (wt%)	Selectivity (%)	Yield (wt%)	Selectivity (%)
C_1-C_6 Compounds				
LG (methane, ethane, propane)	0.27	1.33	0.24	1.68
Ethene	0.45	2.26	0.22	1.54
Propene	2.78	13.97	1.44	10.10
Methylpropene	0.48	2.43	0.37	2.59
Isobutane	2.48	12.47	1.36	9.54
Butane	0.75	3.75	0.41	2.88
Butene	0.42	2.09	0.29	2.03
Methylbutanes	1.60	8.02	0.90	5.68
Methylbutenes	0.11	0.58	0.16	1.12
Pentane	0.15	0.78	0.09	0.63
Pentene	0.02	0.09	0.01	0.07
Methylpentanes	0.49	2.45	0.29	2.03
Methylpentenes	0.04	0.22	0.04	0.28
Methylcyclopentane	0.56	2.78	0.36	2.52
Methylcyclopentene	0.04	0.22	0.03	0.21
Hexane	0.06	0.28	0.03	0.21
Methylhexane	0.14	0.69	0.11	0.77
Cyclohexane	0.04	0.22	0.03	0.21
Cyclohexene	0.14	0.72	0.16	1.12
C_7 Compounds – Paraffins/Olefins				
Heptene	0.10	0.47	0.54	3.79
Heptane	0.22	1.16	0.17	1.19
C_7 Compounds – Isomers				
Dimethylcyclopentane	1.72	8.61	1.10	7.71
Ethylcyclopentane	0.67	3.35	0.51	3.58
Unsaturated Cycloparaffins & Aromatics				
Methylcyclohexene	0.37	1.86	0.42	2.95
Methylcyclohexadiene	0.04	0.20	0.23	1.61
Toluene	2.20	11.06	2.22	15.57
Benzene	0.22	1.09	0.36	2.52
Xylene	0.31	1.57	0.16	1.12
C_8 & C_9 Aromatics	1.84	9.24	0.89	6.32
C8-C9 Compounds				
Dimethylcyclohexanes	0.12	0.61	0.08	0.59
Ethylmethylcyclohexanes	0.02	0.11	0.02	0.14

have provided higher MCH conversions in the case where the reaction rate is influenced by internal mass-transfer limitations. These observations, along with the constant apparent activation energy over the studied temperature range, confirm that MCH is not diffusionally controlled within the crystallite pore network.

This claim is further validated by our research group using model compounds having larger critical diameters than MCH in experiments performed under similar conditions and using the same catalysts.[27,28] In these studies, chemical species with molecule critical diameters in the range of gasoline (i.e., 1,2,4-trimethylbenzene) did not display diffusional limitations under close temperatures, total pressures, and gas-phase concentrations. One should be aware that even if there were mass-transport limitations, diffusion parameters can be assessed independently of adsorption and reaction kinetic parameters using a methodology similar to the one established by Al-Sabawi et al.[26]

Variations in MCH conversions (~2-3%) between the two catalysts can be explained by the differences in their acidity. Although the differences are minor (about 10%), CAT-LC possesses a higher Brønsted-to-Lewis sites ratio than its CAT-SC counterpart, as shown in Table 1. It is well-known that the higher the zeolite acidity, the more cracking exists, because cracking reactions proceed based on a single-site occupancy mechanism.[29] Indeed, more cracking products (C_2-C_6 olefins and paraffins), especially propene and isobutane, were obtained using CAT-LC than CAT-SC. Moreover, while acidity plays a role in providing differences in overall MCH conversion, these differences may also be attributed to the slight variation in BET surface area between the two catalysts (Table 1).

MCH reaction mechanisms

Products formed during MCH conversion were analyzed by GC-MS after each thermal and catalytic cracking experiment. Over 60 product species were detected. Table 2 lists the main species produced and includes the yields obtained at 550°C and 7 s using CAT-LC and CAT-SC.

Based on the different products obtained from MCH conversion, it can be concluded that several types of reactions may take place in the USY zeolite catalysts as follows:

(a) MCH, which has one primary, five secondary and one tertiary carbon atoms, can undergo ring opening and protolytic cracking via secondary and tertiary carbocation intermediates. This mechanism has also been reported in the literature:[30]

Ring Opening/Protolytic Cracking

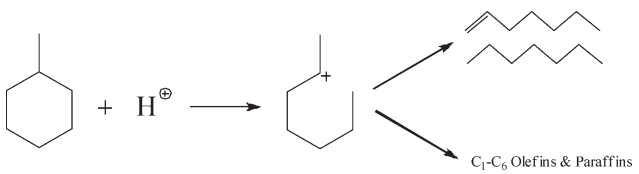

The moderate amounts of heptene and heptane measured in this study, as well as the significant amount of C_1–C_6 hydrocarbons detected (10 wt % using CAT-LC, and 7 wt % using CAT-SC), highlight the importance of this step during MCH conversion.

One should also appreciate that after MCH adsorbs on the catalyst acid site, a carbon-carbon bond may be cleaved resulting in a secondary carbocation. This carbenium ion may return a proton (H^+) back to the catalyst surface and desorb as heptene or may abstract a hydride (H^-) from another molecule and desorb as heptane. Moreover, instead of desorbing as a C_7 hydrocarbon, the carbenium ion may undergo further cracking through β-scission producing smaller C_1-C_6 products.

(b) MCH may experience cracking via β-scission through the following mechanism:[1]

β-scission

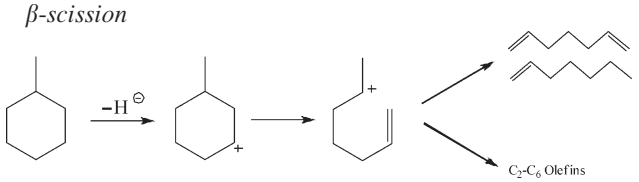

However, no heptadiene was detected among the MCH conversion products, indicating that ring opening of MCH via β-scission may unlikely be a contributing mechanistic step during MCH conversion.

(c) MCH can also isomerize into compounds consisting of 5-carbon ring structures, such as dimethylcyclopentane and ethylcyclopentane. This isomerization process is considered as an important reaction pathway for MCH, as it is widely reported in the literature.[3]

Isomerization

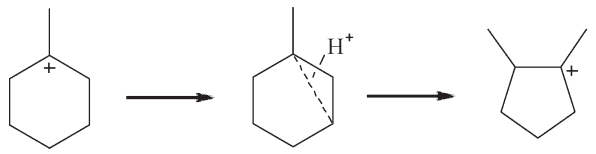

(d) Moreover, the presence of methane, cyclohexene and, to a smaller extent, cyclohexane shows that cleavage of the terminal methyl group of MCH is possible. Cerqueira et al.[3] explains this dealkylation via the following mechanism

Dealkylation

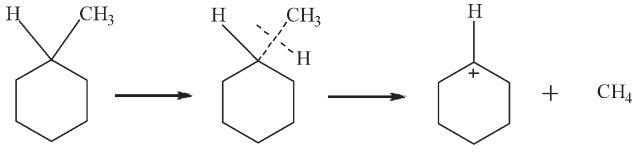

(e) MCH may react via bimolecular hydrogen transfer, contributing to the formation of aromatics as follows[3]

Hydrogen Transfer

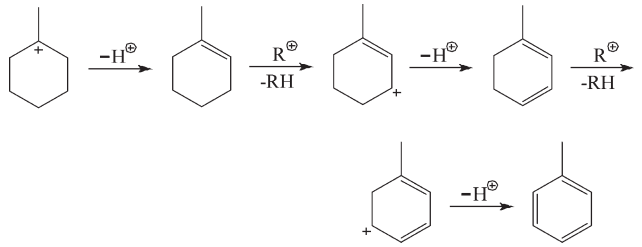

In this study, the data reported in Table 2 shows the presence of unsaturated cycloparaffins, such as methylcyclohexene and methylcyclohexadiene, and the significant amount of aromatic species formed, such as toluene. This indicates that bimolecular hydrogen transfer reactions are prevalent steps during cycloparaffin conversion. In fact, toluene, benzene, xylene and other aromatic compounds make up to 30% of the products formed, by far the highest selectivity out of any of the other classes of product compounds.

(f) Two MCH molecules may react together via transalkylation, a bimolecular process, forming C_8 cycloparaffins such as dimethylcyclohexane and ethylmethylcyclohexane, as follows

Transalkylation

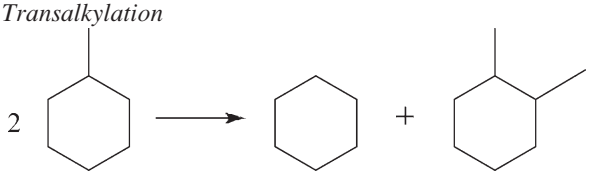

Analysis of the product species of this study shows considerable xylene and C_8 and C_9 aromatics yields. Hence, there is evidence of the contribution of bimolecular transalkylation to the overall MCH conversion scheme.

The development of a kinetic model to describe MCH conversion is a complex process. Thus, taking a practical and effective modeling strategy becomes essential to establish a kinetic model that accurately describes MCH conversion. The approach taken in this study involves the use of observable hydrocarbon product species, as well as MCH reaction mechanisms and pathways, as presented in Figure 6.

Catalyst selectivity results – product yields

To better understand the overall product distribution and MCH reaction mechanisms, the various product yields obtained from the MCH catalytic cracking runs were plotted against MCH conversion.

Ring opening and protolytic cracking of cycloparaffins are important reactions that have been the target of recent studies.[5,6,31] Both CAT-LC and CAT-SC experiments produced a moderate amount of heptenes and heptanes derived from MCH ring opening and a significant amount of C_1 to C_6 hydrocarbons derived from ring carbon-carbon bond cleavage.

Figure 7 reports the C_2-C_6 hydrocarbon yields obtained from experiments conducted with CAT-LC. One can observe that there is a significant amount of cracking products, especially at higher conversions, with the yield reaching 10 wt %. Based on these findings and the reaction mechanism discussed earlier, it can be noticed that C_2-C_6 species are products of secondary reactions, given that MCH ring opening is a necessary first step before smaller hydrocarbon species can be

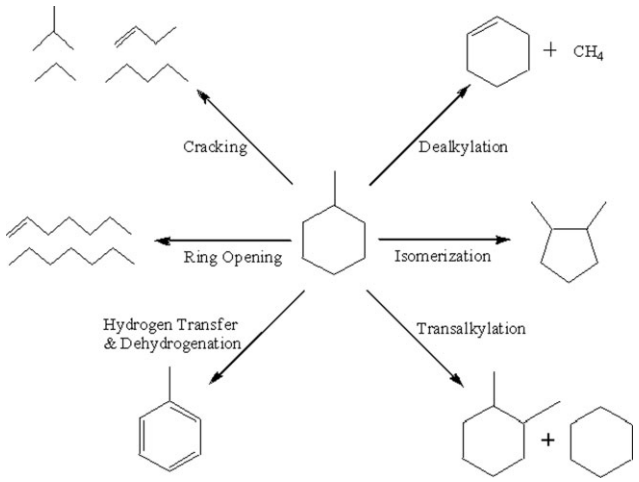

Figure 6. General MCH reactions during FCC.

formed. Hence, one can speculate that C_2-C_6 hydrocarbons come from the protolytic cracking of the methylcyclohexyl carbenium ions or from the over-cracking of primary MCH ring-opening products such as heptene and heptane.

Figure 8 reports the heptene yields over MCH conversions. It can be noticed that the heptene yield starts to stabilize at higher MCH conversions. A similar trend is also observed with heptane. The marked curvature of these plots indicates that both heptene and heptane are consumed in secondary cracking reactions, likely leading to the production of the smaller C_1 to C_6 hydrocarbons.

While it is possible that some heptane may be formed through hydride transfer to a ring-opened carbenium ion, it is expected that most of the heptane is produced via secondary hydrogen transfer reactions of heptene. There were indeed small amounts of heptane detected at low MCH conversion, which may be the result of hydride addition to a carbenium ion with subsequent desorption. It should be pointed out, however, that it is only until there is a considerable amount of heptene formed that the yields of heptane species become significant.

The cracking of heptene or a C_7 ring-opened carbenium ion has been described in the literature to take place in the scheme shown in Figure 9.[32]

Inspection of Table 2 reveals that the most abundant cracking products obtained during MCH conversion were

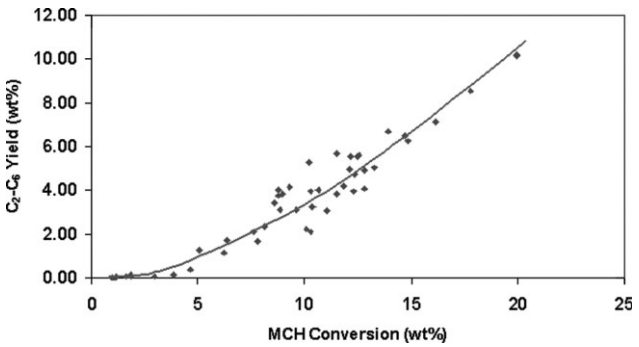

Figure 7. C_2–C_6 yield over MCH conversion using CAT-LC.

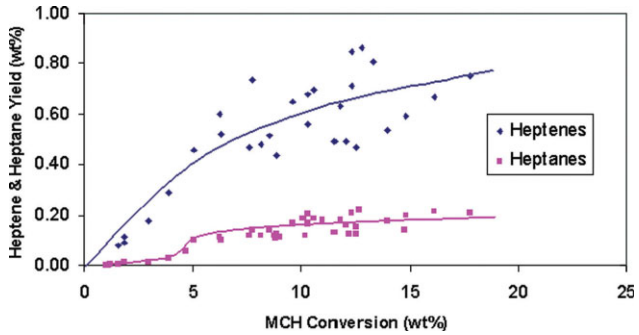

Figure 8. Heptene and heptane yields over MCH conversion using CAT-LC.

[Color figure can be viewed in the online issue, which is available at www.interscience.wiley.com.]

propene and isobutane. These species are likely produced via ring-opened carbenium ions or heptenes converted by the type D β-scission mechanism, as described by Weitkamp et al.[33]. Readsorption of heptene on a Brønsted acid site allows for the formation of a heptyl cation. This cation then may undergo β-scission forming propene and butyl cations. The C_4 carbenium ion may either desorb as n-butene or may abstract a hydride from another molecule, likely a hydrogen donor such as MCH, and desorb as n-butane. As a result, both n-butene and n-butane are found among the reaction products. In any event, once n-butane has been formed, it may isomerize to isobutane.

In addition to ring opening, other primary reactions such as isomerization may take place during MCH catalytic conversion. Figure 10 reports the yield plot for isomerization products of MCH, which includes the yields of dimethylcyclopentanes and ethylcyclopentane. One can notice in this figure a significant initial amount of isomers formed at low MCH conversions. This shows that isomerization reactions are prevalent during cycloparaffin conversion, particularly at low-reaction temperatures. In addition, this figure confirms that isomer production begins to slow down at higher MCH conversions, suggesting that the 5-carbon ring isomers are unstable compounds that may undergo further chemical transformations such ring opening or hydrogen transfer. In fact, McVicker et al.[34] have reported that alkylcyclopentanes can be readily converted at low-temperatures, with the presence of branched paraffins, such as 2-methylhexane (ring opening), as well as the presence of unsaturated 5-carbon ring molecules, such as 3-methylcyclopentene (hydrogen transfer) being an unambiguous indication of this reaction path.

As well, the abundant amount of unsaturated cycloparaffins and aromatics detected among the reaction products highlights the importance and frequency of hydrogen transfer

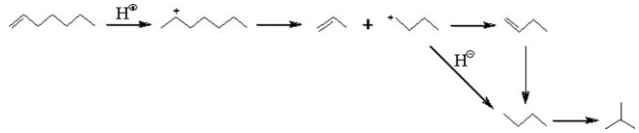

Figure 9. Proposed reaction route for the production of propene and isobutane.

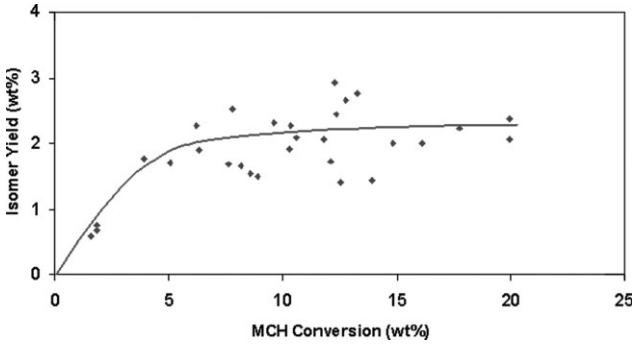

Figure 10. Isomer yield over MCH conversion using CAT-LC.

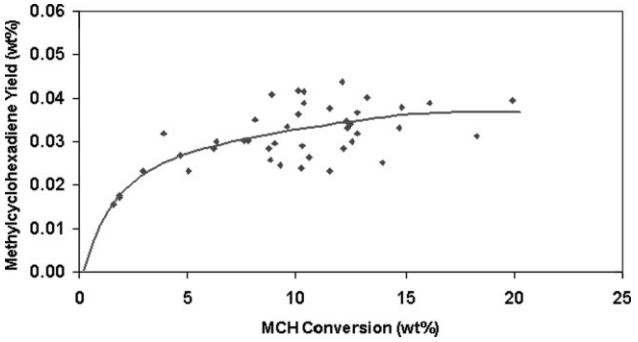

Figure 12. Methylcyclohexadiene yield over MCH conversion using CAT-LC.

during MCH conversion. Even though it takes at least three consecutive bimolecular reactions to form aromatics like toluene, the selectivity of such compounds ranged as high as 24–30%.

As one of the main goals of MCH conversion experiments is to maximize cycloparaffin ring opening and protolytic cracking in order to increase the cetane number,[35,36] a possible approach is to minimize hydrogen-transfer reactions, since the formation of aromatics in gasoline and other refinery products is highly undesirable. Thus, it is in this respect important to determine the extent of hydrogen transfer taking place during MCH experiments. Previous studies[1,3] have reported that during cracking of MCH with zeolites, hydrogen can be transferred from the cycloparaffin feed to the olefins produced by cracking, yielding unsaturated cyclic compounds and eventually, aromatic compounds.

Figures 11 and 12 show the yields of methylcyclohexene and methylcyclohexadiene. These are intermediate unsaturated cyclic compounds, with expected yield plots displaying a significant curvature, thus, indicating that these are unstable products. Although it is expected to see methylcyclohexene at low MCH conversions, it is interesting to observe that methylcyclohexadiene is also present at such low conversions, even though two consecutive bimolecular reactions have to occur to form this hydrocarbon. Since methylcyclohexene is both an olefin and a cycloparaffin, it can behave as either a hydrogen acceptor or hydrogen donor, respectively, and this increases the rate of hydrogen transfer within the catalyst.[1] A possible cause for the significant methylcyclohexene hydrogen transfer is the formation of relatively stable allylic delocalized carbocations.[37] These fast rates of hydrogen transfer can be further favored by the instability of the two unsaturated cycloparaffins, with this leading to the low yields of these species vs. the large amounts of toluene obtained.

Figure 13 reports the yield plot for toluene, displaying an s-shaped curve. The initial part of the yield curve proves that toluene formation requires some reaction time to develop. This is expected as it takes three consecutive bimolecular reaction steps to form this aromatic species. However, one can notice that after a MCH conversion of about 7%, the shape of the yield curve changes, showing that at higher MCH conversions, the toluene becomes consumed by other competing reactions. It is likely that toluene undergoes either dealkylation to form benzene or disproportionation to form both xylene and benzene, as reported in other studies.[3]

Regarding benzene and in clear constrast with toluene, the benzene yield plot displays an exponential shape (Figure 14). This is expected since benzene is a terminal product not undergoing any further chemical transformations. Here again as in the case of toluene, a delay in the production of benzene at lower MCH conversions is observed, since benzene is a secondary product formed from the dealkylation or transalkylation of toluene or alternatively via two consecutive hydrogen-transfer reactions of a dealkylated MCH molecule (cyclohexene). The latter reaction, however, is not significant and only may become prevalent at higher MCH conversions (15 wt %) when the cyclohexene yield plot begins

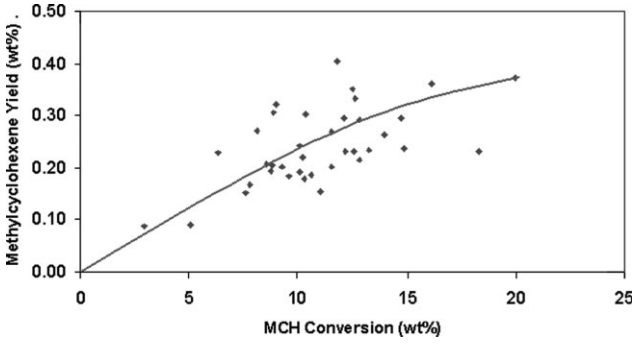

Figure 11. Methylcyclohexene yield over MCH conversion using CAT-LC.

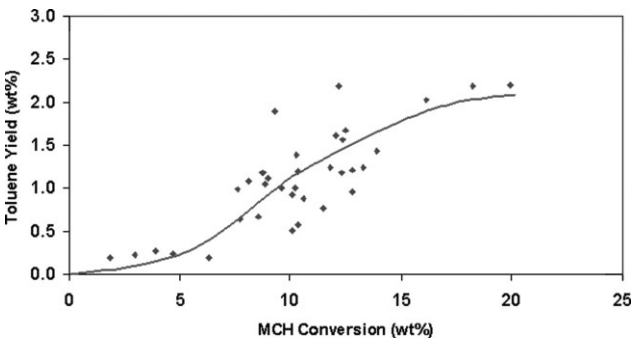

Figure 13. Toluene yield over MCH conversion using CAT-LC.

to plateau (Figure 15), indicating further hydrogen transfer of cyclohexene to cyclohexadiene and finally to benzene.

Figure 14 also shows the similarity of xylene yield results with those of benzene. One can notice that the xylene yield plot has the same shape as the one of benzene, with xylene being, however, the more abundant species even though xylene and benzene are produced in a one-to-one molar ratio via toluene transalkylation. This proves that xylene should be formed via other contributing reactions, namely dehydrogenation or hydrogen transfer of larger C_8 cycloparaffins, which are products of MCH transalkylation. Cerqueira et al.[3] also observed greater amounts of xylene than benzene with all of the zeolite samples tested, arguing that the larger yield of xylenes was due to alkenes aromatization. If this is the case, this would mean that xylene should be produced via the aromatization of C_8 olefins, paraffins or isoparaffins. However, even though aromatization reactions are allowed thermodynamically, none of these hydrocarbon species were detected among the reaction products of this study, which makes this interpretation unlikely to be adequate.[38]

Transalkylation of a methyl group from one MCH molecule to another should take place quite moderately within the zeolite pore network only. This type of reaction leads to the formation of cyclohexanes and C_8 cycloparaffin molecules, such as dimethylcyclohexane and ethylcyclohexane. Since cyclohexane can be also formed via dealkylation of MCH, as well as the hydrogenation of cyclohexene, transalkylation is best measured by determining the C_8 cycloparaffins yield, as reported in Figure 16. As expected, it can be seen that the formation of larger cycloparaffin molecules mainly occurs at low MCH conversions, reaching a 0.25 wt % yield and decreasing later at high MCH conversions. This suggests that C_8 cycloparaffins actively participate in other reactions, particularly hydrogen transfer, forming C_8 aromatics such as xylene, which was observed to be higher in quantity than benzene. This finding is also supported by the significant amounts of other C_8 and even C_9 aromatics found among the reaction products. In this respect, it is important to note that C_8 cycloparaffins do not seem to undergo ring opening, as no octene or octane product species were detected.

Furthermore, the abundant C_8 to C_9 aromatic fraction, while compared with total aromatics, demonstrates that MCH transalkylation products, such as dimethylcyclohexane and ethylcyclohexane, appear to be involved in hydrogen transfer with other cycloparaffins or with olefins, as such types of species are proton acceptors. This is further confirmed by the trend of the C_8 cycloparaffin yield plot in Figure 16, where the amount of C_8–C_9 aromatics is so significant that these species make up almost half the amount of aromatics produced during MCH conversion reactions (Figure 17). This suggests that, due to the confined space within the zeolites, most of the larger molecules stay for a relatively longer time in the catalyst pore network, especially in the longer pores of CAT-LC crystallites.

Thus, based on the observable hydrocarbon products obtained, and based on the analysis of the yield plots, a reaction scheme can be proposed for the catalytic conversion of MCH using USY zeolites in the CREC riser simulator. This reaction scheme is presented in Figure 20, where MCH can undergo several types of reactions, including ring opening, cracking, isomerization, hydrogen transfer, dealkylation and transalkylation.

Modeling Diffusion, Adsorption and Reaction Phenomena

The catalytic cracking of MCH in the mini-fluidized CREC riser simulator is an unsteady-state reaction process. Given that a chemically inert matrix is used in the FCC catalyst, the various chemical reactions can be assumed to take place in the zeolite crystallites only. As a result a material balance of reactant species i in the outer surface of an assumed spherical zeolite crystallite can be written as

$$-\frac{V}{W_{cr}}\frac{dC_{i,ex}}{dt}=\left\{D_{eff,i}\frac{\partial C_{i,in}}{\partial r}\bigg|_{r=R_{cr}}\right\}\frac{3}{R_{cr}\rho_{cr}} \tag{1}$$

where $C_{i,ex}$ and $C_{i,in}$ are the reactant concentration outside and inside the crystallite, respectively, V is the volume of the riser simulator, W_{cr} is the mass of crystallites, ρ_{cr} is the USY zeolite density, R_{cr} is the crystallite radius and D_{eff} is the effective diffusivity of species i in the USY zeolite pore network.

Modeling of the cracking reaction, as given in Eq. 1, has to be complemented by a partial differential equation in the assumed spherical zeolite crystallite as follows

$$(K_i\rho_{cr}+\varepsilon)\frac{\partial C_{i,in}}{\partial t}+\frac{D_{eff,i}}{r^2}\frac{\partial}{\partial r}\left(r^2\frac{\partial C_{i,in}}{\partial r}\right)=\rho_{cr}(r_i) \tag{2}$$

where r_i is the rate of consumption/formation of species i, ε the crystallite voidage, and K_i the adsorption constant for species i.

Furthermore, a number of initial boundary conditions are required for modeling catalytic cracking of MCH in the CREC riser simulator. These include

1. Instantaneous vaporization of all chemical species ($t = 0$, $C_{i,ex}=C_{i,ex}|_{t=0}$);
2. Symmetric concentration profiles inside the crystallites ($r = 0$, $\partial C_{i,in}/\partial r = 0$);
3. Negligible transport limitations around the 60 μm particles and inside the inert matrix ($r = R_c$, $C_{i,in} = C_{i,ex}$).

Conditions (1) and (3) can be fully satisfied under the operating conditions of the CREC riser simulator, whereas condition (2) can be validated by the crystallite shape with all three dimensions being of comparable magnitude.[39]

Solving Eqs. 1 and 2 numerically helps demonstrate that the accumulation term on the lefthand side of Eq. 2 is negligible for reactions with reaction times of 3, 5, and 7 s. This consideration was proven to be valid by Al-Khattaf and de Lasa[40] for reaction times greater than 2 s. Thus, under these conditions, a "quasi-steady state" effectiveness factor, η_{ss}, which accounts for diffusion of reactant species through the zeolite pore network, can be defined as

$$\eta_{ss}=\frac{r_{mean}}{-k_iC_{i,in}^1\big|_{r=R_{cr}}} \tag{3}$$

where k_i is the intrinsic kinetic constant and r_{mean} is the observed rate of consumption/formation.

Furthermore, under "quasi-steady state" conditions and combining Eqs. 1, 2 and 3, the disappearance of MCH in the

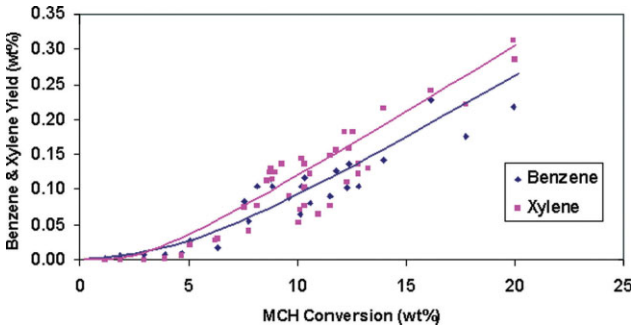

Figure 14. Benzene and xylene yields over MCH conversion using CAT-LC.

[Color figure can be viewed in the online issue, which is available at www.interscience.wiley.com.]

well-mixed mini-fluidized CREC riser simulator can be represented by the following species balance equation

$$\frac{V}{W_{cr}}\frac{dC_A}{dt} = \eta_{ss} r_A \tag{4}$$

where r_A is the rate of the consumption of MCH in the absence of diffusion control and C_A represents the concentration of MCH in the gas phase.

The proposed model, as given by Eqs. 2, 3 and 4, is adequate in the CREC riser simulator considering: (a) the high-gas recirculation;[25] (b) the intensively-fluidized catalyst securing uniform catalyst activity (constant coke distribution) throughout the bed at a given retention time;[21] and (c) the catalytic reaction limited to the zeolite given the inert catalyst matrix used in this study.[24]

Based on observable product species obtained during catalytic experiments, the product yield plots presented in Figures 7 to 17, and the reaction scheme reported in Figure 18, a simplified kinetic model that accurately describes MCH catalytic conversion may be developed, as presented in Figure 19. This model considers primary reactions, including:

(a) Ring opening and cracking of MCH into heptene and olefins with seven carbons or less;

(b) Isomerization of MCH into 5-carbon ring compounds, including ethylcyclopentane and dimethylcyclopentane;

(c) Dealkylation of MCH, forming cyclohexene and methane; and

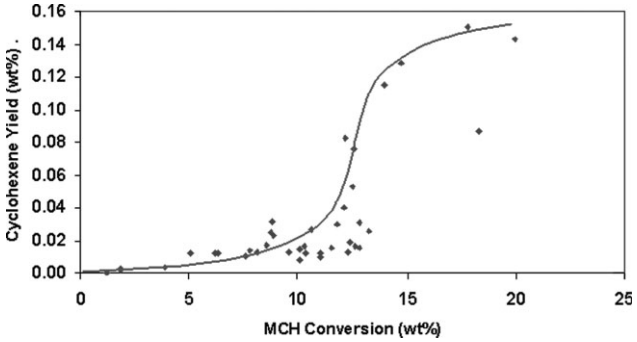

Figure 15. Cyclohexene yield over MCH conversion using CAT-LC.

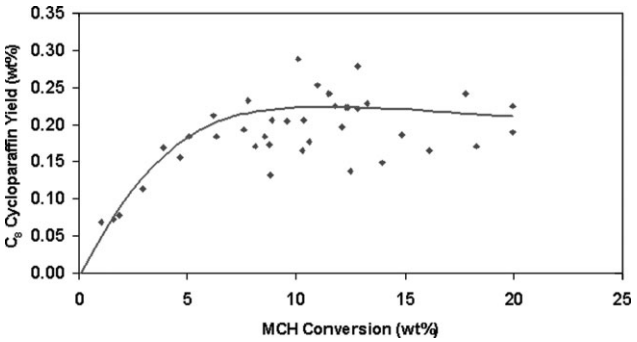

Figure 16. C_8 cycloparaffins yield over MCH conversion using CAT-LC.

(d) Transalkylation of MCH into larger C_8 and C_9 cycloparaffins.

In addition, given the significant of amounts of aromatics formed, such as toluene, benzene, xylene and other C_8 and C_9 aromatic compounds, it becomes necessary to include four other secondary reactions in the proposed model:

1. Hydrogen transfer between MCH and olefins resulting in the hydrogenation of olefins into paraffins and the unsaturation of MCH into methylcyclohexene, methylcyclohexadiene and toluene;

2. Hydrogen transfer between cyclohexene and olefins, resulting in the formation of benzene and paraffins.

3. Hydrogen transfer between C_8 and C_9 cycloparaffins and olefins leading to the production C_8 and C_9 aromatics and paraffins; and

4. Transalkylation of toluene to produce benzene and xylene (this reaction was incorporated in the kinetic model due to the apparent consumption of toluene, which was observed in Figure 13);

MCH conversion through reactions (a), (b) and (c) are modeled via rate equations displaying first-order kinetics in the numerator of the rate equation, since the kinetic order of cracking single molecules is unity[41] and since all of these types of reactions are unimolecular. Trans-alkylation and hydrogen-transfer reactions, on the other hand, described by reactions (d), (1), (2), (3) and (4) are modeled by second-order kinetics, since two molecules are involved in these reaction steps. In addition, every reaction step includes a

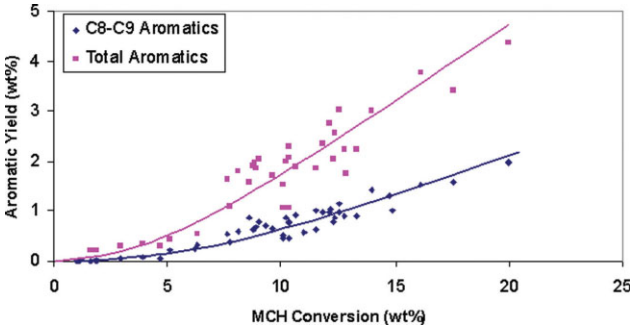

Figure 17. Yield of C_8-C_9 aromatics and total aromatics over MCH conversion using CAT-LC.

[Color figure can be viewed in the online issue, which is available at www.interscience.wiley.com.]

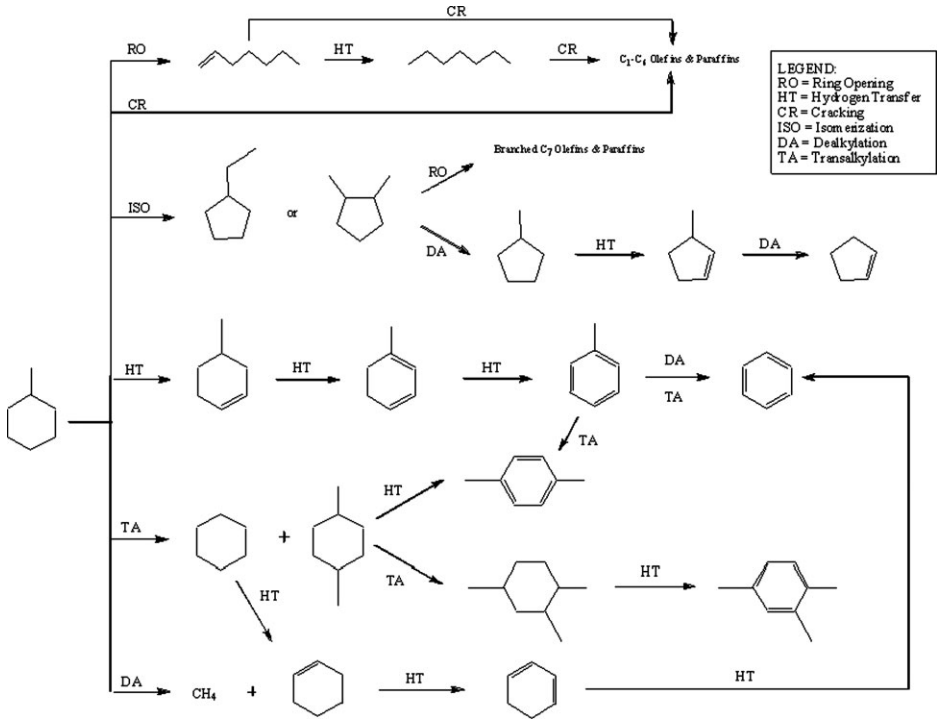

Figure 18. Simplified reaction scheme for the catalytic cracking of MCH based on observable products.

denominator in the rate equation accounting for adsorption, as can be expected in the case of catalytic reactions following Hinselwood-Langmuir formulations.

It is also important to consider the influence of thermal cracking during catalytic cracking runs. As previously discussed, thermal effects play a role in the conversion of MCH. To establish the extent of thermal cracking in overall MCH conversion, thermal cracking products were analyzed using the GC. As expected, the majority of the primary reaction products formed via catalytic steps (cracking, ring opening, isomerization, dealkylation) were also present in the case of thermal cracking (Figure 20). However, transalkylation and hydrogen transfer bimolecular reactions that usually require the presence of a catalyst were considered to be very limited and therefore, were not included in the overall thermal conversion reaction model.

As a result of accounting for both catalytic and thermal cracking (Figures 19 and 20), the following equation can be considered for cracking of MCH in the CREC riser simulator

$$-V\frac{dC_A}{dt} = \eta_{ss}\varphi_{\text{int}}W_{cr} \times \left[\begin{array}{l} \dfrac{K_A}{1+K_AC_A}(k_1+k_2+k_3)C_A \\ +\dfrac{2K_A}{(1+K_AC_A)^2}k_4C_4^2+\dfrac{K_AK_B}{(1+K_AC_A+K_BC_B)^2}k_5C_AC_B \end{array}\right] + Vk_{T1,2,3}C_A \quad (5)$$

where k_1, k_2, k_3, k_4, and k_5 are the intrinsic kinetic constant, associated with the reactions shown in Figure 19, $k_{T1,2,3}$ is the overall thermal intrinsic kinetic constant associated with the MCH thermal cracking which combines all thermal constants presented in Figure 20, K_A and K_B represent the adsorption constants for MCH and olefins, respectively, and φ_{int} is the catalyst activity decay function.

Moreover, if one considers the concentration of MCH, C_A, and olefins C_B, in the CREC riser simulator, a reactor of constant volume, species concentrations can be related at any reaction time to their mass fractions y_A and y_B, by

$$C_A = \frac{y_AW_{hc}}{MW_AV} \quad \text{and} \quad C_B = \frac{y_BW_{hc}}{MW_BV} \quad (6)$$

where W_{hc} is the total mass of hydrocarbons injected in the riser simulator, while MW_A and MW_B are the molecular weights of MCH and the olefin products, respectively. The value of MW_B was determined based on the yield and molecular weight of each type of olefin formed.

Thus, the consumption of MCH in the CREC riser simulator can be evaluated in terms of mass fractions using the following equation

$$-V\frac{dy_A}{dt} = \eta_{ss}\varphi_{\text{int}}W_{cr} \times \left[\begin{array}{l} \dfrac{K_A}{1+K_AC_A}(k_1+k_2+k_3)y_A \\ +\dfrac{2\alpha K_A}{(1+K_AC_A)^2}k_4y_A^2+\dfrac{\beta K_AK_B}{(1+K_AC_A+K_BC_B)^2}k_5y_Ay_B \end{array}\right] + Vk_{T1,2,3}y_A \quad (7)$$

where $\alpha = \left(\frac{W_{hc}}{MW_AV}\right)$ and $\beta = \left(\frac{W_{hc}}{MW_BV}\right)$

Furthermore, each thermal and catalytic intrinsic kinetic constant k_i, can be postulated to change with the reactor temperature T, following a reparameterized Arrhenius-type equation

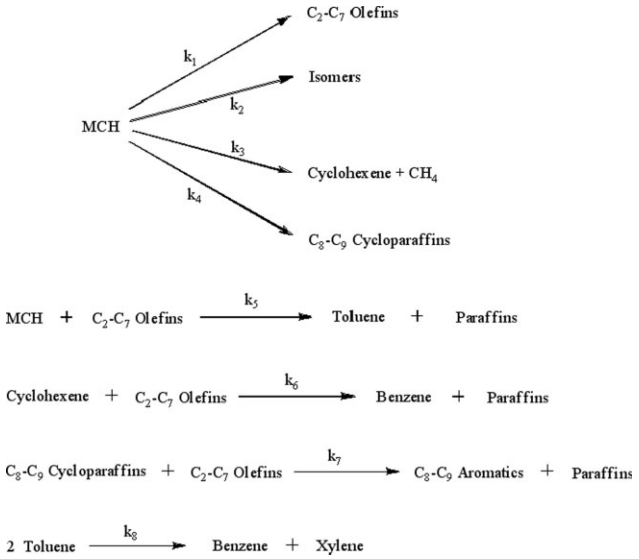

Figure 19. Proposed MCH catalytic conversion model.

$$k_i = k_{i0} \exp\left(\frac{-E_i}{R}\left(\frac{1}{T} - \frac{1}{T_0}\right)\right) \tag{8}$$

where E_i represents the energy of activation, k_{i0} is the pre-exponential factor, and T_0 is the centering temperature defined as the average temperature used in the reaction experiments, which is 500°C.

Moreover, one can also argue on the basis of adsorption thermodynamics that each adsorption constant for species i is exponentially related to the corresponding reaction temperature as

$$K_i = K_{i0} \exp\left(\frac{-\Delta H_i}{RT}\right) \tag{9}$$

where K_{i0} is the pre-exponential factor with units of m^3/(kg of catalyst), and ΔH_i is the heat of adsorption in kJ/mol. Performing thermal and catalytic experiments in a range of temperatures and using Eq. 9 allows for the independent assessment of adsorption parameters, as will be discussed later.

It is well-known that the deposition of coke on the catalyst surface decreases the catalyst activity, since coke covers the active sites of the catalyst. Catalyst activity decay function φ_{int}, can be accounted for relating catalyst activity to the coke concentration on the catalyst, as suggested by Froment and Bischoff.[42] Thus, φ_{int} can be evaluated by the following expression

$$\varphi_{\text{int}} = \exp(-\lambda X'_{coke}) \tag{10}$$

where λ is the deactivation parameter for MCH cracking, and X'_{coke} represents the mass of coke produced per mass of MCH injected. This kinetic model does not consider the effect of coke on adsorption processes. Adsorption parameters are not assumed to depend on the amount of coke produced. This assumption is based on results published by Atias et al.[43] who found that adsorption constants and available surface area remain somewhat constant at low levels of coke. Coke analysis will be discussed in the modeling section of this article.

Similarly, chemical species balances can be established for the other products both in terms of species concentrations and weight fractions, with these balances containing formation and/or consumption of chemical species.

Olefins (B)

$$V\frac{dC_B}{dt} = \eta_{ss}\varphi_{\text{int}}W_{cr} \times \left[\frac{K_A}{1+K_AC_A}k_1C_A - \frac{K_AK_B}{(1+K_AC_A+K_BC_B)^2}k_5C_AC_B - \frac{K_BK_D}{(1+K_BC_B+K_DC_D)^2}k_6C_BC_D - \frac{K_BK_E}{(1+K_BC_B+K_EC_E)^2}k_7C_BC_E\right] + Vk_{T1}C_A \tag{11}$$

$$V\frac{dy_B}{dt} = \eta_{ss}\varphi_{\text{int}}W_{cr} \times \left[\frac{v_BK_A}{1+K_AC_A}k_1y_A - \frac{\alpha K_AK_B}{(1+K_AC_A+K_BC_B)^2}k_5y_Ay_B - \frac{\alpha K_BK_D}{(1+K_BC_B+K_DC_D)^2}k_6y_By_D - \frac{\delta K_BK_E}{(1+K_BC_B+K_EC_E)^2}k_7y_By_E\right] + v_BVk_{T1}y_A \tag{12}$$

where $v_B = \left(\frac{MW_B}{MW_A}\right)$, $\sigma = \left(\frac{W_{bc}}{MW_DV}\right)$ and $\delta = \left(\frac{W_{bc}}{MW_EV}\right)$.

Isomers (C)

$$V\frac{dC_C}{dt} = \eta_{ss}\varphi_{\text{int}}W_{cr}\frac{K_A}{1+K_AC_A}k_2C_A + Vk_{T2}C_A \tag{13}$$

$$V\frac{dy_C}{dt} = \eta_{ss}\varphi_{\text{int}}W_{cr}\frac{v_CK_A}{1+K_AC_A}k_2y_A + v_CVk_{T2}y_A \tag{14}$$

where $v_C = \left(\frac{MW_C}{MW_A}\right)$.

Cyclohexene (D)

$$V\frac{dC_D}{dt} = \eta_{ss}\varphi_{\text{int}}W_{cr} \times \left[\frac{K_A}{1+K_AC_A}k_3C_A - \frac{K_BK_D}{(1+K_BC_B+K_DC_D)^2}k_6C_BC_D\right] + Vk_{T3}C_A \tag{15}$$

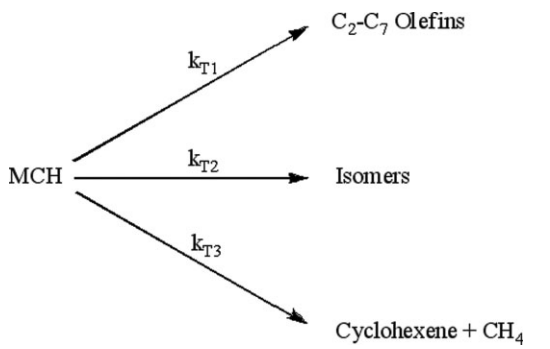

Figure 20. Proposed MCH thermal conversion model.

$$V\frac{dy_D}{dt} = \eta_{ss}\varphi_{\text{int}}W_{cr} \times \left[\frac{v_D K_A}{1+K_A C_A}k_3 y_A - \frac{\beta\, K_B K_D}{(1+K_B C_B + K_D C_D)^2}k_6 y_B y_D\right] + v_D V k_{T3} y_A \quad (16)$$

where $v_D = \left(\frac{MW_D}{MW_A}\right)$.

C_8-C_9 Cycloparaffins (E)

$$V\frac{dC_E}{dt} = \eta_{ss}\varphi_{\text{int}}W_{cr}\left[2\frac{K_A}{(1+K_A C_A)^2}k_4 C_A^2 - \frac{K_B K_E}{(1+K_B C_B + K_E C_E)^2}k_7 C_B C_E\right] \quad (17)$$

$$V\frac{dy_E}{dt} = \eta_{ss}\varphi_{\text{int}}W_{cr}\left[2\frac{\alpha v_E K_A}{(1+K_A C_A)^2}k_4 y_A^2 - \frac{\beta K_B K_E}{(1+K_B C_B + K_E C_E)^2}k_7 y_B y_E\right] \quad (18)$$

where $v_E = \left(\frac{MW_E}{MW_A}\right)$.

Toluene (F)

$$V\frac{dC_F}{dt} = \eta_{ss}\varphi_{\text{int}}W_{cr}\left[\frac{K_A K_B}{(1+K_A C_A + K_B C_B)^2}k_5 C_A C_B - 2\frac{K_F}{(1+K_F C_F)^2}k_8 C_F^2\right] \quad (19)$$

$$V\frac{dy_F}{dt} = \eta_{ss}\varphi_{\text{int}}W_{cr}\left[\frac{\beta v_F K_A K_B}{(1+K_A C_A + K_B C_B)^2}k_5 y_A y_B - 2\frac{\gamma\, K_F}{(1+K_F C_F)^2}k_8 y_F^2\right] \quad (20)$$

where $v_F = \left(\frac{MW_F}{MW_A}\right)$ and $\gamma = \left(\frac{W_{hc}}{MW_F V}\right)$.

Benzene (G)

$$V\frac{dC_G}{dt} = \eta_{ss}\varphi_{\text{int}}W_{cr}\left[\frac{K_B K_D}{(1+K_B C_B + K_D C_D)^2}k_6 C_B C_D + 2\frac{K_F}{(1+K_F C_F)^2}k_8 C_F^2\right] \quad (21)$$

$$V\frac{dy_G}{dt} = \eta_{ss}\varphi_{\text{int}}W_{cr}\left[\frac{\sigma\, v_G K_B K_D}{v_B(1+K_B C_B + K_D C_D)^2}k_6 y_B y_D + 2\frac{\gamma\, v_G K_F}{v_F(1+K_F C_F)^2}k_8 y_F^2\right] \quad (22)$$

where $v_G = \left(\frac{MW_G}{MW_A}\right)$.

C_8-C_9 Aromatics (H)

$$V\frac{dC_H}{dt} = \eta_{ss}\varphi_{\text{int}}W_{cr}\frac{K_B K_E}{(1+K_B C_B + K_E C_E)^2}k_7 C_B C_E \quad (23)$$

$$V\frac{dy_H}{dt} = \eta_{ss}\varphi_{\text{int}}W_{cr}\frac{\beta\, v_H K_B K_E}{v_E(1+K_B C_B + K_E C_E)^2}k_7 y_B y_E \quad (24)$$

where $v_H = \left(\frac{MW_H}{MW_A}\right)$.

Xylene (I)

$$V\frac{dC_I}{dt} = 2\eta_{ss}\varphi_{\text{int}}W_{cr}\frac{K_F}{(1+K_F C_F)^2}k_8 C_F^2 \quad (25)$$

$$V\frac{dy_I}{dt} = 2\eta_{ss}\varphi_{\text{int}}W_{cr}\frac{\gamma\, v_I K_F}{v_F(1+K_F C_F)^2}k_8 y_F^2 \quad (26)$$

where MW_C, MW_D, MW_E, MW_F, MW_G, MW_H and MW_I are the average molecular weights for MCH isomers, cyclohexene, C_8-C_9 cycloparaffins, toluene, benzene, C_8-C_9 aromatics and xylene, respectively.

Thus, the thermal and catalytic conversion of MCH in the CREC riser simulator can be modeled using Eqs. 7 to 10, 12, 14, 16, 18, 20, 22, 24 and 26, with these equations factoring in both adsorption and reaction phenomena.

Assessment of Adsorption Parameters in the CREC Riser Simulator

A set of thermal and catalytic experiments at various temperatures were performed to assess the adsorption parameters of MCH on typical FCC catalysts. The adsorption constants of MCH were experimentally calculated from the pressure profiles recorded during experiments carried out with and without catalyst loaded in the CREC riser simulator. Comparing the pressure attained at the end of the vaporization period for a thermal and a catalytic experiment (point "B" in Figure 1), the difference between pressures represents the fraction of reactant adsorbed on the catalyst.

In a thermal run, the total mass of reactant species i injected is simply equal to the mass of species i in the gas phase

$$m_{i,injected} = m_{i,gas}^{thermal} \quad (27)$$

On the other hand, in a catalytic run, the total mass of reactant species i injected becomes vaporized and is distributed between the gas phase and the adsorbed phase

$$m_{i,injected} = m_{i,gas}^{catalytic} + m_{i,catalyst} \quad (28)$$

Hence, by comparing thermal and catalytic runs carried out under the same reaction conditions, the mass of reactants adsorbed on the catalyst can be calculated by

$$m_{i,catalyst} = m_{i,gas}^{thermal} - m_{i,gas}^{catalytic} \quad (29)$$

where $m_{i,gas}$ (thermal) is the mass of species i for the thermal run at the time of complete vaporization, and $m_{i,gas}$ (catalytic) is the mass of species i in the gas phase for a catalytic reaction at the time of complete vaporization (point B in Figure 1). This equation may also be expressed in terms of pressures using the ideal gas law, since a low-total pressure range is used in this study (15–40 psia)

$$m_{i,catalyst} = \frac{\left(P_i^{thermal} - P_i^{catalyst}\right) V\, MW_i}{RT} \tag{30}$$

Rearranging Eq. 30, the number of moles of species i adsorbed on the catalyst $n_{i,catalyst}$, is

$$n_{i,catalyst} = \frac{\left(P_i^{thermal} - P_i^{catalyst}\right) V}{RT} \tag{31}$$

Moreover, the concentration of species i adsorbed on the catalyst surface q_i, can be defined considering the ratio of the number of moles of species i adsorbed to the mass of catalyst m_{cat}, as follows

$$q_i = \frac{n_{i,catalyst}}{m_{cat}} = \frac{\left(P_i^{thermal} - P_i^{catalyst}\right) V/RT}{m_{cat}} \tag{32}$$

Furthermore, under the relatively low-pressure conditions of FCC, MCH adsorption at equilibrium is expected to display a linear isotherm,[43] similar to Henry's law

$$q_i = K_i C_i \tag{33}$$

where K_i is the adsorption constant of species i and C_i is the concentration of species i in the vapor phase. Thus, adsorption of chemical species at equilibrium under FCC reaction conditions can be represented using a relationship analogous to Henry's law.[43] The high-temperatures of FCC gas-phase reactions cause reactant hydrocarbon species to occupy only a relatively small fraction of adsorption sites on the catalyst, and this low coverage of the available surface area within the catalyst validates the use of a linear relationship to model adsorption.[43]

Since the concentration of species i in the vapor phase C_i, by definition is

$$C_i = \frac{m_{i,gas}^{catalytic}}{MW_i \cdot V} = \frac{\left(P_i^{catalytic} - P_{atm}\right)}{RT} \tag{34}$$

The adsorption constant of species i in Henry's law can be isolated and expressed in terms of Eqs. 32 and 34. The result is the following simplified equation

$$K_i = \frac{\left(P_i^{thermal} - P_i^{catalytic}\right) V}{\left(P_i^{catalytic} - P_{atm}\right) m_{cat}} \tag{35}$$

where $P_i^{thermal}$ and $P_i^{catalytic}$ are the total pressure at the moment of vaporization (point "B" in Figure 1) for the thermal and the catalytic experiments, respectively, P_{atm} is the initial pressure (= 14.7 psia), and V is the volume of the CREC riser simulator reactor.

Equation 35 allows the calculation of adsorption constants at initial conditions of the catalytic reaction as a decoupled calculation of the kinetic parameters. Therefore, assessment of adsorption constants through Eq. 35 requires pressure profiles of both the thermal and the catalytic runs under the same conditions.

The assumptions behind the derivation of Eq. 35 are the following:

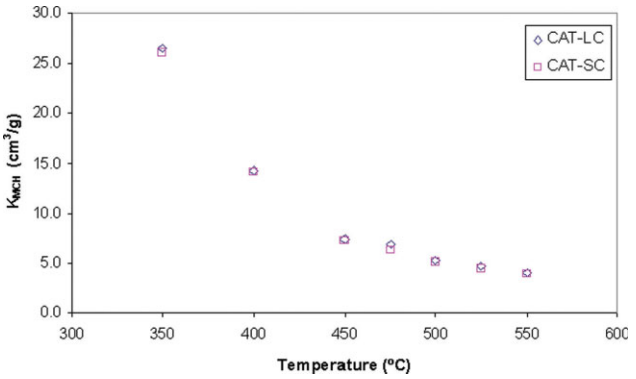

Figure 21. Adsorption constants for MCH at different temperatures over CAT-LC and CAT-SC.

[Color figure can be viewed in the online issue, which is available at www.interscience.wiley.com.]

(a) Adsorption/desorption quasi-equilibrium conditions are reached and occur rapidly compared to the time required for the overall transport.

(b) The reactant molecule does not have hindered mobility through the pore network of the catalyst. This is a condition that can be used for MCH.

(c) The total mass of reactant species i injected is immediately vaporized and can be considered equal to the mass of species i in the gas phase (thermal experiments), or distributed between the gas and adsorbed phase (catalytic experiments).

(d) Ideal gas law holds given the operating conditions of low-total pressure employed in this study (15–40 psia) and high-temperatures (350–550°C).

(e) Adsorption of MCH on USY zeolite crystallites under the high-temperature and low-relative pressure conditions is considered to follow a linear isotherm, similar to the Henry's law as given by Eq. 33.

Adsorption constants for MCH were evaluated at different temperatures, ranging from 350 to 550°C for both the CAT-LC and CAT-SC catalysts. This approach and the use of Eq. 9 allows for the assessment of the heat of adsorption using a linear regression technique. A centering temperature T_0 (723 K) was used to assess parameters with low cross-correlation. Figure 21 reports adsorption constants for MCH over two FCC catalysts, CAT-LC and CAT-SC, at various temperatures. Given the exothermic nature of adsorption, and the relationship shown in Eq. 9, the adsorption constants are expected to decrease with temperature. This in fact was the case, as pressure differences between conditions of loaded and unloaded catalyst, as given by Eq. 35, decreased with temperature.

It is important to note that due to the relatively small magnitude of the adsorption constants for the temperature range of this study (450–550°C), the value of $K_A C_A$ becomes much smaller than 1 (i.e., $K_A C_A \ll 1$), since $K_A C_A = 0.02$ at 550°C, and 0.05 at 450°C. Note that in this case, K_A is in m^3/mol, and C_A is in mol/m^3. Therefore, the Langmuir-Hinselwood representation of the adsorption discussed earlier $K_A/(1 + K_A C_A)$, can be simplified to K_A in the overall rate equation for the conversion of MCH (Eq. 7), as well as in rate Eqs. 12, 14, 16, 18 and 20.

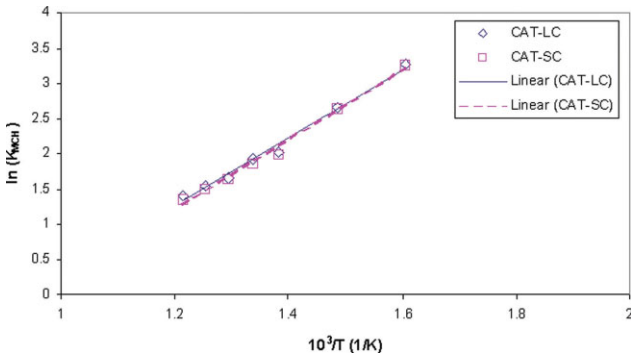

Figure 22. Arrhenius plot for MCH over CAT-LC and CAT-SC.

[Color figure can be viewed in the online issue, which is available at www.interscience.wiley.com.]

Figure 22 displays the K_i Arrhenius plot for MCH. The heats of adsorption were found to be −40.30 and −41.37 kJ/mol for CAT-LC and CAT-SC, respectively (Table 3). These negative and similar heats of adsorption reflect the exothermic nature of the adsorption and the similarity of adsorption phenomena in the two zeolites studied.

In order to evaluate the intrinsic kinetic parameters of the proposed catalytic cracking model included in Eqs. 7, 12, 16, 20, 22, 24 and 26, it is essential to calculate adsorption constants for C_2-C_7 olefins (K_B), cyclohexene (K_D), C_8-C_9 cycloparaffins (K_E), and toluene (K_F) products. Calculation of these constants allows for the ability to decouple adsorption parameters from kinetic parameters and, consequently, adsorption and reaction phenomena can be assessed independently.

The same method used to calculate K_A was considered to determine K_B, K_D, K_E, and K_F adsorption constants. Although there are several olefin compounds formed via the ring opening or β-scission of MCH, k_B was evaluated using heptene. As for k_E, it is approximated using xylene, a C_8 aromatic. Although xylene is not a cycloparaffin, the adsorption parameters of a naphthene and an aromatic compound having the same carbon number will be very similar, since adsorption constants are mainly related to compound molecular weight.[44] In fact, this similarity is observed in the adsorption constants obtained for MCH and toluene, a naphthene and an aromatic with the same carbon number (C_7).

Table 4 presents olefin (heptene), cyclohexene, xylene and toluene adsorption constants evaluated at 450°C. The magnitudes of these constants are relatively smaller that the adsorption constant of MCH. Moreover, the sum of $(K_AC_A + K_BC_B)$ and $(K_BC_B + K_DC_D)$ is much smaller than 1. This allows for another simplification to the model equations containing the $K_AK_B/(1 + K_AC_A + K_BC_B)^2$ and $K_BK_D/(1 + K_BC_B + K_DC_D)^2$ terms, using instead $K_A K_B$ and $K_B K_D$ respectively.

Table 3. Heats of Adsorption and Adsorption Constants for MCH over CAT-LC and CAT-SC

	CAT-LC	CAT-SC
$K_{A0} \times 10^6$ [m^3/(kg of catalyst)]	10.35 ± 0.58	8.44 ± 0.80
ΔH_A (kJ/mol)	−40.30 ± 2.26	−41.37 ± 3.98

Table 4. Adsorption Constants for MCH Conversion Products Participating in Secondary Reactions

	Adsorption Constant @ 450°C [m^3/(kg of crystallite)] ± 15%	Heat of Adsorption (kJ/mol) ± 15%
Olefins (Heptene)	0.00151	−29.0
Cyclohexene	0.00251	−51.8
Xylene	0.02565	−51.8
Toluene	0.02278	−48.5

The values were obtained using CAT-LC.

Evaluation of Intrinsic Kinetic Parameters

Modeling results – thermal cracking parameters

During a catalytic cracking experiment, most of the converted MCH reactant molecules are transformed into products with the help of a catalyst (catalytic cracking), while some may be converted as a result of thermal effects (thermal cracking). In most kinetic studies,[9,40] the effect of thermal cracking is a minor one and, as a result, kinetic models usually do not incorporate thermal kinetic parameters. In this study, however, it has been shown that thermal effects are significant and cannot be ignored. Thus, thermal kinetic parameters were included in the proposed model presented earlier. These will be evaluated in this section.

Determination of the thermal kinetic constants (pre-exponential factors k_{T1}, k_{T2}, k_{T3}, and activation energies E_{T1}, E_{T2}, E_{T3}) can be approached as an independent exercise from the evaluation of the other model parameters, particularly the intrinsic catalytic kinetic parameters. In fact, thermal conversion of MCH in the CREC riser simulator can be described by the simplified form of Eq. 7, considering only the thermal effects

$$-\frac{dy_A}{dt} = k_{T1,2,3}y_A \tag{36}$$

where $k_{T1,2,3} = k_{T1} + k_{T2} + k_{T3}$, and k_{T1}, k_{T2} and k_{T3} are the thermal intrinsic kinetic constant, associated with MCH ring opening/cracking, isomerization and dealkylation, respectively, as shown in Figure 20.

Equations for the formation of products during thermal conversion experiments can also be expressed as follows

$$\text{Heptene/Olefins:}\quad \frac{dy_B}{dt} = v_B k_{T1} y_A \tag{37}$$

$$\text{Isomers:}\quad \frac{dy_C}{dt} = v_C k_{T2} y_A \tag{38}$$

$$\text{Cyclohexene:}\quad \frac{dy_D}{dt} = v_D k_{T3} y_A \tag{39}$$

Applying nonlinear regression to data (yields of each product and unconverted MCH) obtained from thermal runs in the riser simulator, along with Eqs. 8 and 36 to 39, allows for the independent evaluation of six thermal cracking kinetic constants from other model parameters. These thermal constants are reported in Table 5.

Table 5. Kinetic Parameters for MCH Thermal Conversion

	Value	95% CFL
k_{T10} (1/s)	0.0889	0.0058
E_{T1} (kJ/mol)	68.80	12.00
k_{T20} (1/s)	0.0148	0.0038
E_{T2} (kJ/mol)	50.28	44.44
k_{T30} (1/s)	0.0215	0.0043
E_{T3} (kJ/mol)	42.75	33.71

It is important to note that a two-step process was carried out in the evaluation of these six parameters. First, the values of each pair of thermal kinetic parameters (k_{Ti0}, E_{Ti}) were determined independently from the other two pairs. These values were then used as initial guesses when all six parameters of the complete thermal model were evaluated simultaneously.

The correlation matrix obtained for thermal cracking parameters, presented in Table 6, shows little cross-correlation between the fitted parameters, and this statistically describes the low level of interaction between the calculated parameters. Moreover, analysis of residual distribution, model-predicted values, and experimental data points in Figure 23 shows a regular distribution of residuals with no prediction bias, thus, proving the adequacy of the fitted parameters.

Modeling results – catalytic cracking parameters

Given that the adsorption parameters (K_{A0} and ΔH_A) and (K_{B0}, K_{D0}, K_{E0}, K_{F0}, ΔH_B, ΔH_D, ΔH_E, ΔH_F), as well as the intrinsic thermal kinetic parameters (k_{T1}, k_{T2}, k_{T3}, E_{T1}, E_{T2}, E_{T3}) were already calculated in previous sections of this study, intrinsic catalytic kinetic parameters ($k_{10} - k_{80}$, $E_1 - E_8$ and λ) need to be assessed to fully characterize the adsorptive-reactive system. This sequential methodology of parameter estimation leads to adsorption parameters with smaller spans than the intrinsic kinetic parameters because of the propagation of errors.

As previously mentioned, the overall rate of MCH conversion is controlled via intrinsic kinetic, and it is not hindered by MCH diffusion within the USY crystallites. Therefore, the effectiveness factor term, initially included in the proposed modeling equations to factor in the diffusion phenomenon, was set equal to one.

The amount of coke deposited on the catalyst active sites was measured using a total organic carbon (TOC) analyzer. It was determined that, under worst-case reaction conditions (i.e., at highest reaction temperature (550°C), and longest reaction time (7 s)), coke levels were quite low, measuring

Table 6. Cross-Correlation Matrix for Nonlinear Regression of Experimental Data Collected During Thermal Cracking of MCH

	k_{T10}	E_{T1}	k_{T20}	E_{T2}	k_{T30}	E_{T3}
k_{T10}	1	−0.47	−0.42	0.16	−0.51	0.18
E_{T1}	−0.47	1	0.15	−0.42	0.16	−0.51
k_{T20}	−0.42	0.15	1	−0.27	−0.20	0.05
E_{T2}	0.16	−0.42	−0.27	1	0.04	−0.20
k_{T30}	−0.51	0.16	−0.20	0.04	1	−0.18
E_{T3}	0.18	−0.51	0.05	−0.20	−0.18	1

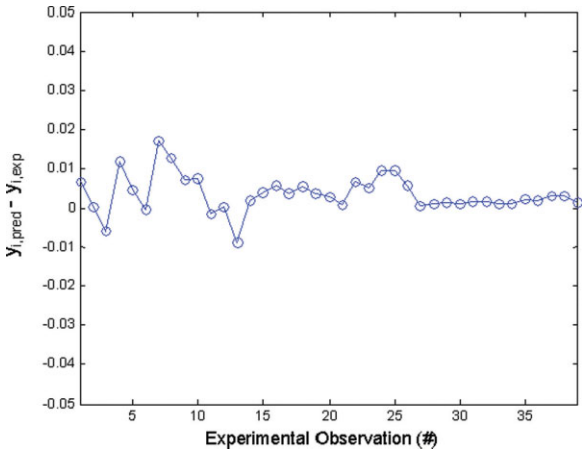

Figure 23. Residual distribution for nonlinear regression of data obtained during MCH thermal cracking runs in the CREC riser simulator.

[Color figure can be viewed in the online issue, which is available at www.interscience.wiley.com.]

at 0.29 wt %. Since coke yields obtained under all other experimental conditions were less than this amount, the deactivation parameter λ was considered to be negligible for modeling purposes.

Following these simplifications, the proposed catalytic cracking kinetic model including 16 intrinsic catalytic kinetic parameters was assessed. These parameters were evaluated using nonlinear regression of the experimental data of MCH conversions at temperatures ranging from 450 to 550°C, and at reaction times of 3, 5 and 7 s. The function of residuals was minimized using the large-scale algorithm based on the interior-reflective Newton method described in Coleman and Li.[45]

In order to reduce the number of parameters evaluated simultaneously and to decrease possible fitting errors, the model proposed in Figure 19 was divided into four smaller and distinctive reaction models: (1) MCH isomerization (k_{20}, E_2); (2) MCH ring-opening/cracking, MCH transalkylation and hydrogen transfer to form large aromatics (k_{10}, E_1, k_{40}, E_4, k_{70}, E_7); (3) MCH dealkylation and hydrogen transfer to form benzene (k_{30}, E_3, k_{60}, E_6); and (4) formation and consumption of toluene (k_{50}, E_5, k_{80}, E_8). With this approach, the maximum number of parameters to be evaluated at one time was six. This "split model" is referred to as model #1.

After completing this initial parameter evaluation, the complete model in Figure 19 with all of its 16 kinetic parameters was solved at once (referred to as model #2). The model parameter values obtained using the two methods were compared in order to establish the accuracy of the solution of the 16-parameter model. Table 7 reports the intrinsic kinetic parameters obtained using CAT-LC along with the corresponding 95% confidence limits. This table includes the kinetic parameters calculated using each of the two methods (i.e., model #1 and model #2) along with percent difference between them.

Despite the large number of intrinsic parameters included in the proposed kinetic model, one can see that solving the 16 parameters simultaneously (model #2) is almost as precise as evaluating the parameters of model #1 (Table 7). With the exception of a few parameters only (i.e., k_{60}, k_{80},

Table 7. Intrinsic Kinetic Parameters for MCH Catalytic Conversion over CAT-LC

	Model #1		Model #2		% Difference
	Value	95% CFL	Value	95% CFL	Between Methods
k_{10} (1/s)	8.813	0.100	6.741	0.077	23.5
E_1 (kJ/mol)	78.29	1.53	73.78	1.44	5.8
k_{20} (1/s)	6.917	0.210	2.218	0.055	67.9
E_2 (kJ/mol)	68.08	3.87	49.55	2.24	27.2
k_{30} (1/s)	0.623	0.137	0.386	0.084	38.0
E_3 (kJ/mol)	101.21	35.37	53.61	19.69	47.0
k_{40} (m^3/mol/s)	0.048	0.001	0.016	0.001	66.1
E_4 (kJ/mol)	67.72	3.66	73.50	8.46	−8.5
k_{50} (1/mol/s)	4.105×10^8	1.613×10^7	1.779×10^8	9.498×10^6	56.6
E_5 (kJ/mol)	57.78	6.72	81.33	6.94	−40.8
k_{60} (1/mol/s)	2.330×10^{11}	9.253×10^{10}	2.507×10^{12}	1.311×10^{12}	−975.6
E_6 (kJ/mol)	91.84	71.43	113.01	37.01	−23.1
k_{70} (1/mol/s)	3.364×10^{10}	2.460×10^9	3.103×10^{10}	4.442×10^9	7.8
E_7 (kJ/mol)	64.67	8.72	87.64	21.18	−35.5
k_{80} (1/mol/s)	6.915×10^8	1.239×10^8	1.378×10^8	4.251×10^7	80.1
E_8 (kJ/mol)	56.17	28.22	10.83	44.07	80.17

E_8), most percent differences between the parameters obtained using the two methods were reasonable. This result confirms that the 16-parameter model was solved accurately. Moreover, the correlation matrix obtained for catalytic cracking parameters in model #2 showed extremely low cross-correlation between the fitted parameters and this statistically confirmed the low level of interaction between the calculated parameters (Table 8).

In addition, analysis of residual distribution, model-predicted values, and experimental data points in Figure 24 showed a regular distribution of residuals with no prediction bias, thus, proving the adequacy of the fitted parameters.

It is also important to note that most of the 95% confidence limits calculated for each parameter were moderate (<39%), indicating that the fittings obtained were accurate. However, the 95% confidence interval of the activation energy associated with the transalkylation of toluene (i.e., E_8) was greater than the calculated value of this parameter, indicating that the kinetic constant k_8, is statistically insignificant and may be eliminated from the model. This observation shows that disproportionation of toluene into benzene and xylene is minor and that toluene is involved in other reactions that allow for its consumption, as observed by the shape of the yield curve in Figure 13. Toluene may in fact experience dealkylation instead of transalkylation to form benzene. This matter is discussed further in the upcoming section of this study.

A comparison of the intrinsic activation energies values for primary MCH reactions determined that the catalytic cracking and ring opening of a MCH molecule involves a higher energy of activation than isomerization: 74 vs. 50 kJ/mol. Thus, an increase in temperature leads to a larger fraction of heptene and smaller cracking products, as illustrated in Figures 25a and 26a. The lower activation energies reported for the isomerization of MCH show that isomerization reactions are less sensitive to temperature variations. Thus, isomer formation does not change significantly with temperature, as will be confirmed in the next section of this study.

Comparing the intrinsic activation energies of the reactions involved in both the thermal and catalytic models, it is apparent that the values of these parameters are very similar and the differences between them are statistically insignificant. For instance, the catalytic activation energies for ring-

Table 8. Cross-Correlation between Kinetic Constants of the 16-Parameter Model

	k_{10}	E_{10}	k_{20}	E_{20}	k_{30}	E_{30}	k_{40}	E_{40}	k_{50}	E_{50}	k_{60}	E_{60}	k_{70}	E_7	k_{80}	E_8
k_{10}	1	−0.21	−0.37	−0.02	−0.23	0.04	−0.21	0.04	−0.18	0.06	0.04	0	0.10	0.01	0.28	0.09
E_{10}	−0.21	1	0	−0.32	0.04	−0.26	0.05	−0.18	0.06	−0.27	0	0	0	0.08	−0.01	0.16
k_{20}	−0.37	0	1	0.22	−0.09	0	−0.13	−0.03	−0.04	0.01	0.03	0	−0.02	0.01	0.03	0.02
E_{20}	−0.02	−0.32	0.22	1	−0.01	−0.07	−0.02	−0.24	−0.01	0.03	−0.01	0.07	0.01	−0.03	0.02	0
k_{30}	−0.23	0.04	−0.09	−0.01	1	−0.14	−0.24	0	−0.10	0.03	0.06	−0.01	0.10	−0.15	0.05	0.04
E_{30}	0.04	−0.26	0	−0.07	−0.14	1	0	−0.22	0.03	−0.14	0	0.03	−0.15	0.18	0.01	−0.01
k_{40}	−0.21	0.05	−0.13	−0.02	−0.24	0	1	0.11	−0.48	0.07	−0.44	0.06	−0.08	0.04	−0.38	−0.24
E_{40}	0.04	−0.18	−0.03	−0.24	0	−0.22	0.11	1	0.03	−0.34	0.03	−0.35	0.04	−0.09	−0.09	−0.08
k_{50}	−0.18	0.06	−0.04	−0.01	−0.10	0.03	−0.48	0.03	1	−0.37	0.35	−0.13	−0.02	0.03	0.14	0.15
E_{50}	0.06	−0.27	0.01	0.03	0.03	−0.14	0.07	−0.34	−0.37	1	−0.14	0.30	0.03	−0.05	0.02	−0.09
k_{60}	0.04	0	0.03	−0.01	0.06	0	−0.44	0.03	0.35	−0.14	1	−0.40	0.01	−0.01	0.01	0.11
E_{60}	0	0	0	0.07	−0.01	0.03	0.06	−0.35	−0.13	0.30	−0.40	1	−0.01	0.01	0.03	−0.15
k_{70}	0.10	0	−0.02	0.01	0.10	−0.15	−0.08	0.04	−0.02	0.03	0.01	−0.01	1	−0.36	0.04	0.03
E_7	0.01	0.08	0.01	−0.03	−0.15	0.18	0.04	−0.09	0.03	−0.05	−0.01	0.01	−0.36	1	0	0
k_{80}	0.28	−0.01	0.03	0.02	0.05	0.01	−0.38	−0.09	0.14	0.02	0.01	0.03	0.04	0	1	0.55
E_8	0.09	0.16	0.02	0	0.04	−0.01	−0.24	−0.08	0.15	−0.09	0.11	−0.15	0.03	0	0.55	1

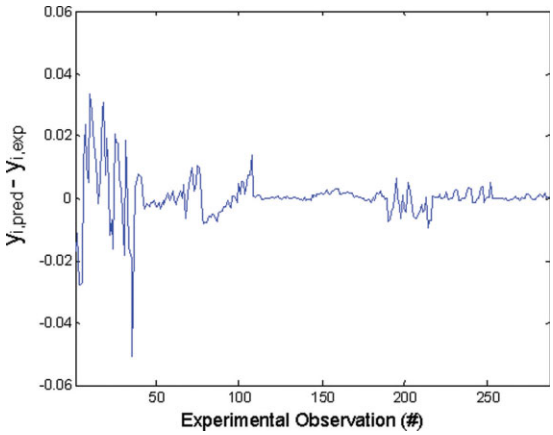

Figure 24. Residual distribution for nonlinear regression of data obtained using CAT-LC (16-Parameter Model).

[Color figure can be viewed in the online issue, which is available at www.interscience.wiley.com.]

opening/cracking, isomerization and dealkylation reactions were 74, 50 and 54 kJ/mol, respectively, and the thermal activation energies for the same reactions were 69, 50 and 43 kJ/mol, respectively. This confirms the accuracy of the parameter fitting exercise, as intrinsic activation energy values for the same reactions should be identical. It is the apparent activation energies that should be different between thermal and catalytic conversion. Addition of the catalytic intrinsic activation energy values to the heats of adsorption assessed earlier for MCH (−40 kJ/mol) yields apparent energies of activation ranging from 10–34 kJ/mol. Hence, these values are much lower than those of thermal conversion, as expected.

Modeling results – product yields

Once the 10 adsorption parameters, as well as the 22 thermal and catalytic kinetic parameters were determined, the distributions of the reaction products were calculated by solving the set of Eqs. 7, 12, 14, 16, 18, 20, 22, 24, and 26. Figures 25 and 26 illustrate the product distributions as a function of MCH conversion at 450 and 550°C, respectively. These simulated distributions differ from the experimental yield plots presented earlier in the section entitled "Catalyst selectivity results-product yields", as they provide product yields over a span of reaction times at a fixed reaction temperature. Such plots are preferred by people in the FCC industry.

The product distribution plots show that, under most conditions, ring opening/cracking, hydrogen transfer and isomerization are the predominant primary reactions during MCH conversion. The rate of dealkylation, on the other hand, seems to be the smallest, and this is confirmed by the relatively low cyclohexene yields obtained in cracking experiments.

There are major differences in product yields when comparing the yields plots obtained at low-and high-reaction temperatures. For instance, it is apparent that the rate of ring-opening/cracking increases drastically with temperature. For instance, the olefin yield increases from 2.6 wt % to 3.7 wt % at a MCH overall conversion of 16 wt %. This is not surprising, as the energy of activation associated with ring-opening/cracking was relatively high (74 kJ/mol). The lower amount of olefins produced at 450°C compared to 550°C is due to (1) the promotion of ring-opening and protolytic cracking rates at high-temperatures, and (2) the greater mass-transport restrictions that product species experience as they leave the zeolite pore network under lower-reaction temperatures. As olefins diffuse out of the catalyst pores under low-reaction temperatures, there is an increased possibility that they will interact with hydrogen donor species, such as naphthenes, leading to hydrogen transfer reactions. As a result, the olefin yield curve should stabilize to indicate olefin consumption to paraffins and, in addition, the aromatic selectivity should be higher at 450°C. Indeed, both of these results are observed. The aromatic yield (sum of yields of toluene, benzene and C_8-C_9 aromatics) is 3.5 wt % at

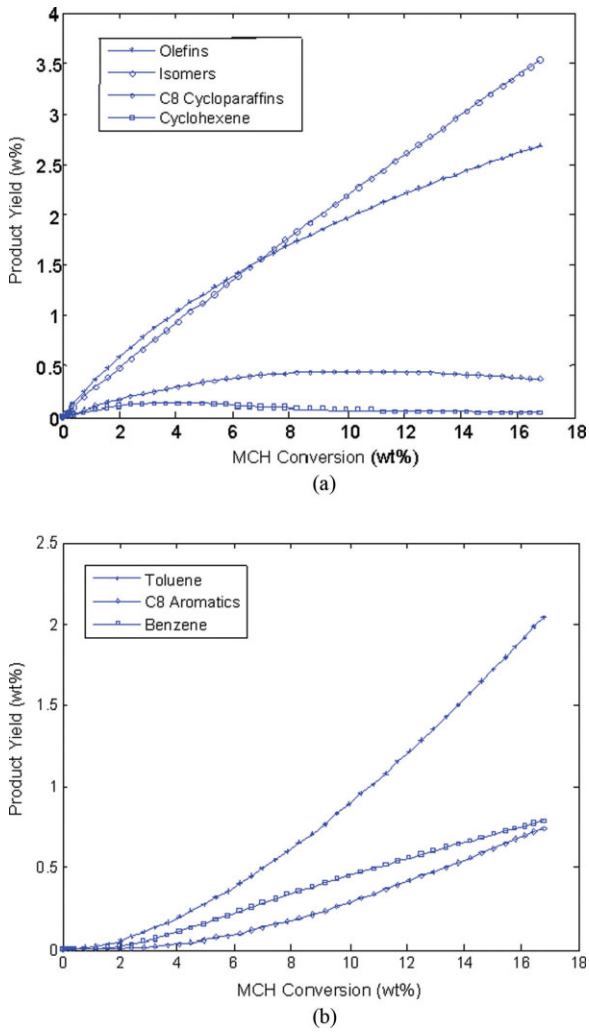

Figure 25. Selectivity of (a) primary products obtained using CAT-LC at a temperature of 450°C. (b) secondary products (aromatics) obtained using CAT-LC at a temperature of 450°C.

[Color figure can be viewed in the online issue, which is available at www.interscience.wiley.com.]

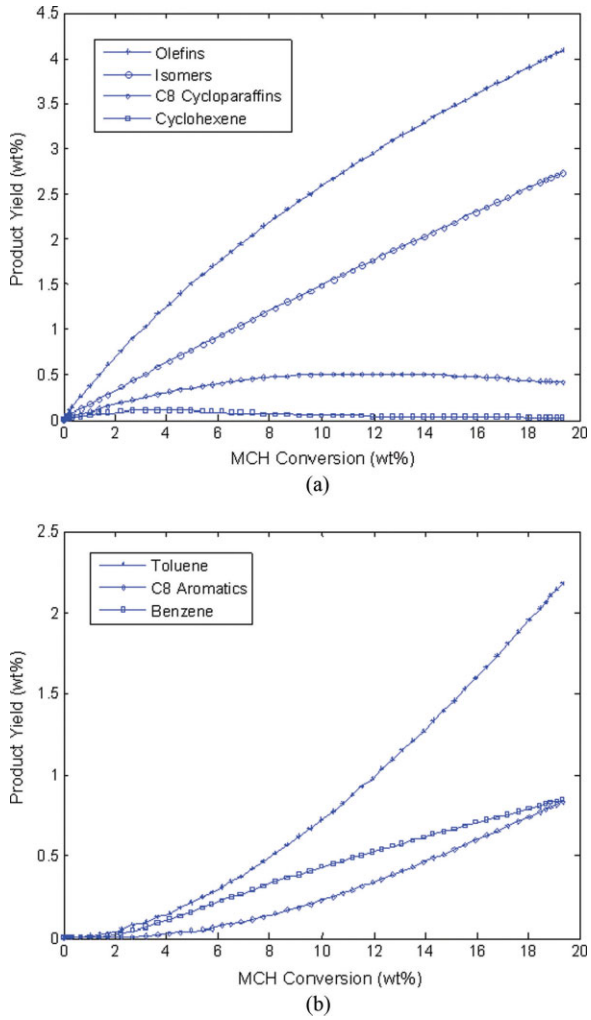

Figure 26. Selectivity of (a) primary products obtained using CAT-LC at a temperature of 550°C; (b) secondary products (aromatics) obtained using CAT-LC at a temperature of 550°C.

[Color figure can be viewed in the online issue, which is available at www.interscience.wiley.com.]

450°C vs. 2.9 wt % at 550°C when the MCH conversion is 16 wt %.

Regarding aromatic compounds, it can be noticed that slightly more benzene is produced at lower-temperatures (0.8 wt % at 450°C vs. 0.7 wt % at 550°C). This can also be attributed to hindrance that product molecules experience in the long pores of the larger zeolite crystallites at lower-temperatures. In this case, toluene may not be able to leave the catalyst pore network early enough to avoid undergoing dealkylation into benzene. Although toluene transalkylation may also be possible, it was shown earlier that the kinetic constant associated with such a reaction was trivial.

The same explanation can be given for the higher C_8-C_9 aromatics obtained at 450°C. The diffusional limitations that products like C_8-C_9 cycloparaffins experience allow them to continue to react to form their complementary aromatics.

Moreover, the toluene yields are 2.0 wt % and 1.6 wt % at 16 wt % MCH conversion at 450 and 550°C, respectively. Thus, based on the higher yields attained for aromatics at 450°C vs. 550°C for a particular MCH conversion, if can be concluded that hydrogen-transfer reactions are more pronounced and selectively favored against other reactions, such as cracking, at lower-reaction temperatures.[29]

As for isomer production, it was noticed that the yields did not change considerably with temperature. This is supported by Kubicka et al.[6] who also observed that temperature does not seem to affect isomer distribution during cycloparaffin conversion.

Conclusion

The contributions of this manuscript can be summarized as follows:

(a) Slightly higher overall MCH conversions were obtained using CAT-LC vs. CAT-SC, and these differences are attributed to the both the small difference in acidity of the catalysts, as well as the higher rate of hydrogen-transfer reactions taking place within the crystallites of CAT-LC, since the diffusional pathways are longer in these crystallites.

(b) Reaction pathways of MCH and its products were determined, confirming those proposed by previous studies conducted outside FCC conditions.

(c) A heterogeneous kinetic model for the catalytic cracking of MCH describing thermal effects, as well as adsorption and reaction phenomena, applicable in the context of the CREC riser simulator, was established.

(d) Kinetic parameters, including thermal and primary catalytic intrinsic activation energies, were determined using nonlinear regression and statistical parameter estimation techniques. Calculated parameters were in the range of 43–69 kJ/mol and 50–74 kJ/mol, respectively.

(e) Adsorption constants for MCH on USY zeolite catalyst were assessed under typical catalytic cracking reaction conditions. The exothermic nature of MCH adsorption was confirmed, given the − 40 kJ/mol heat of adsorption.

(f) MCH conversion was proven to take place without diffusional limitations under relevant FCC conditions. This finding is due to the small critical molecular size of MCH, providing relatively easy molecular penetration through the zeolite catalyst pore network.

(g) It was found that ring-opening/cracking, hydrogen transfer and isomerization are more dominant primary reactions during MCH conversion compared to other reactions, such as dealkylation and transalkylation. This finding was supported on the basis of the main products formed: C_2-C_7 olefins, aromatics and MCH isomers with 5-member carbon rings.

(h) It was observed that hydrogen-transfer reactions were favored against other reactions at lower-temperatures, whereas ring-opening/cracking reactions predominated at higher-temperatures.

Acknowledgements

The authors are very appreciative for the financial support provided by in The National Centre of Upgrading Technology (NCUT) and for

the Canada Graduate Scholarship (CGS) provided by the Natural Sciences and Engineering Research Council of Canada (NSERC) to Mr. Mustafa Al-Sabawi.

Notation

C_i = concentration of species i in the vapor phase, mol/m^3
$C_{i,ex}$ = concentration of species i outside the USY crystallite, mol/m^3
$C_{i,in}$ = concentration of species i within the pore network of the USY crystallite, mol/m^3
D_{eff} = effective diffusivity, m^2/s
E_i = intrinsic activation energy catalytic reaction i, kJ/mol
E_{Ti} = intrinsic activation energy for thermal reaction i, kJ/mol
K_i = adsorption constant for species i [m^3/(kg of catalyst)]
K_{i0} = adsorption pre-exponential factor [m^3/(kg of catalyst)]
k_i = intrinsic kinetic constant for catalytic reaction i (s^{-1}) or [m^3/(mol·s)] or [1/(mol·s)]
k_{i0} = pre-exponential factor for catalytic reaction i (s^{-1}) or [m^3/(mol·s)] or [1/(mol·s)]
k_{Ti} = intrinsic kinetic constant for thermal reaction i (s^{-1})
k_{Ti0} = pre-exponential factor for thermal reaction i (s^{-1})
MW_i = molecular weight of species I, kg/mol
p_i = partial pressure of species I, KPa
$q_{i,in}$ = molar concentration of species i adsorbed inside the crystallite, mol/kg
R_{cr} = radius of zeolite crystallite (m), or universal gas constant [J/(K·mol)]
r = radial coordinate, m
r_i = kinetic rate of consumption/formation of species i {mol/[$kg_{crystallite}$·s]}
r_{mean} = observed rate of consumption/formation {mol/[$kg_{crystallite}$·s]}
T = reactor temperature, K
T_0 = average temperature of experiments, 773.15K
t = reaction time, s
V = volume of the riser simulator, m^3
W_{cr} = mass of crystallites, kg
W_{hc} = total mass of hydrocarbons inside the riser, kg
X_E = mass of coke produced per mass of gas oil injected, kg_{coke}/kg_{MCH}
y_i = mass fraction of species i in the vapor phase
$y_{i,pred}$ = mass fraction of species i in the vapor phase predicted by kinetic model

Greek letters

ε = USY crystallite porosity
ΔH_i = heat of adsorption of species i, kJ/mol
φ_{int} = intrinsic catalyst activity decay function
η_{ss} = effectiveness factor
ρ_{cr} = density of the USY zeolite crystallite, kg/m^3
v_i = stoichiometric coefficient for species i, calculated as MW_A/MW_i
λ = deactivation parameter, RC model

Subscripts

A = MCH
B = olefins
C = isomers
D = cyclohexene
E = C_8-C_9 cycloparaffins
F = toluene
G = benzene
H = C_8-C_9 Aromatics
I = xylene

Abbreviations

CAT-LC = catalyst prepared with large zeolite crystallites
CAT-SC = catalyst prepared with small zeolite crystallites
CFL = confidence limit
C/O = catalyst-to-oil ratio, $kg_{catalyst}$/kg_{MCH}

Literature Cited

1. Corma A, Mocholi F, Orchilles V, Koemer GS, Madon RJ. Methylcyclohexane and methylcyclohexene cracking over zeolite Y catalysts. *Appl Catal, A*. 1991;67:307–324.
2. Corma A, Gonzalez-Alfaro V, Orchilles AV. Decalin and Tetralin as probe molecules for cracking and hydrotreating the light cycle oil. *J Catal*. 2001;200:34–44.
3. Cerqueira HS, Mihindou-Koumba PC, Magnoux P, Guisnet M. Methylcyclohexane transformation over HFAU, HBEA and HMFI zeolites: I. Reaction scheme and mechanisms. *Ind Eng Chem Res*. 2001;40:1032–1041.
4. Mostad HB, Riis TU, Ellestad OH. Catalytic cracking of naphthenes and naphtheno-aromatics in fixed bed micro reactors. *Appl Catal, A*. 1990;63:345–364.
5. Kubicka D, Kumar N, Maki-Arvela P, Tiitta M, Niemi V, Salmi T, Murzin DY. Ring opening of decalin over zeolites I: Activity and selectivity of proton-form zeolites. *J Catal*. 2004a;222:65–79.
6. Kubicka D, Kumar N, Maki-Arvela P, Tiitta M, Niemi V, Salmi T, Murzin DY. Ring opening of decalin over zeolites II: Activity and selectivity of platinum-modified zeolites. *J Catal*. 2004b;227:313–327.
7. Sadegbeigi R. *Fluid catalytic Cracking: Design, Operation, and Troubleshooting of FCC Facilities*. Houston: Gulf Publishing Company; 2000.
8. Bhatia S. *Zeolite Catalysis: Principles and Applications*. Boca Raton: CRC Press, Inc.; 1990.
9. Atias J, de Lasa H. Adsorption and catalytic reaction over FCC catalysts in a novel fluidized CREC riser simulator. *Chem Eng Sci*. 2004;59:5663–5669.
10. Do DD. *Adsorption Analysis: Equilibria and Kinetics*. London, U.K: Imperial College Press; 1998.
11. Hershkowitz F, Madiara P. Simultaneous measurements of adsorption, reaction and coke using a pulsed microbalance reactor. *Ind Eng Chem Res*. 1993;32:2969–2974.
12. Weisz PB. Molecular diffusion in microporous materials: formalisms and mechanisms. *Ind Eng Chem Res*. 1995;34:2692–2699.
13. Chmelka BF, Pearsons JG, Liu SB, Ryoo R, de Menorval LC, Pines AJ. NMR study of the distribution of aromatic molecules in NaY zeolite. *J Phys Chem*. 1991;95:303–310.
14. Murzin D, Salmi T, Smeds S, Laatikainen M, Mustonen M, Paatero E. Toluene and methylcyclohexane adsorption on nickel catalysts. *React Kinet Catal Lett*. 1997;61:227–236.
15. Thamm H, Stach H, Fiebig W. Calorimetric Study of the Absorption of n-Butane and But-l-ene on a Highly Dealuminated Y-type Zeolite and on Silicalite. *Zeolites*. 1983;3:95–97.
16. Jänchen J, Stach H. Dependence of the adsorption equilibrium of n-decane on the Si/Al-ratio of faujasite zeolites. *Zeolites*. 1985;5:57–59.
17. Stach H, Thamm J, Jänchen J, Fiedler R, Schirmer W. *Experimental and Theoretical Investigations of the Adsorption of n-Paraffins, Olefins and Aromatics in Zeolites*. Proceedings of the Sixth International Zeolite Conference. Olson D, Bisio A, eds. Butterworths: Guildford, U.K; 1984:225–231.
18. Denayer JFM, Baron GV. Adsorption of normal and branched paraffins in faujasite zeolites NaY, HY, Pt/NaY and USY. *Adsorption*. 1997;3:251–265.
19. Atkinson DG. Curthoys. Heats and entropies of adsorption of saturated hydrocarbons on zeolites X and Y. J. *Chem Soc Faraday Trans*. 1981;I77:897–907.
20. Corma A, Ortega FJ. Influence of adsorption parameters on catalytic cracking and catalyst decay. *J Catal*. 2005;233:257–265.
21. de Lasa HI. Riser Simulator for Catalytic Cracking Studies. 1991. U.S. Patent #5,102,628.
22. de la Puente G, Devard A, Sedran U. Conversion of residual feedstocks in fcc. evaluation of feedstock reactivity and product distributions in the laboratory. *Energy Fuels*. 2007;21:3090–3094.
23. Arandes JM, Azkoiti MJ, Torre I, Olazar M Castano P. Effect of HZSM-5 Catalyst addition on the cracking of polyolefin pyrolysis waxes under fcc conditions. *Chem Eng J*. 2007;132:17–26.
24. Tonetto G, Atias JA, de Lasa H. FCC catalysts with different zeolite crystallite sizes: acidity, structural properties and reactivity. *Appl Catal A*. 2004;270:9–25.
25. Ginsburg JM, Pekediz A, de Lasa HI. The CREC fluidized riser simulator: characterization of mixing patterns. *Int J Chem Reactor Eng*. 2003;1(A-52):1–12.

26. Al-Sabawi M, Atias JA, de Lasa H. Kinetic modeling of catalytic cracking of gas oil feedstocks: reaction and diffusion phenomena. *Ind Eng Chem Res*. 2006;45:1583–1593.
27. Atias JA, Tonetto G, de Lasa HI. Catalytic conversion of 1,2,4-trimethylbenzene in a crec riser simulator. A heterogeneous model with adsorption and reaction phenomena. *Ind Eng Chem Res*. 2003;42:4162–4173.
28. Atias JA, de Lasa H. Adsorption and catalytic reaction in fcc catalysts using a novel fluidized CREC riser simulator. *Chem Eng Sci*. 2004;59:5663–5669.
29. de la Puente G, Sedran U. Conversion of methylcyclopentane on rare earth exchanged Y zeolite FCC catalysts. *Appl Catal*. 1996;144:147–158.
30. Wojciechowski B, Corma A. *Catalytic Cracking*. New York: Marcel Dekker; 1986.
31. Santikunaporn M, Herrera JE, Jongpatiwut S, Resasco D, Alvarez WE, Sughrue EL. Ring opening of decalin and tetralin on HY and Pt/HY zeolite catalysts. *J Catalysis*. 2004;228:100–113.
32. Buchanan J, Santiesteban J, Haag W. Mechanistic considerations in acid-catalyzed cracking of olefins. *J Catalysis*. 1996;158:279–287.
33. Weitkamp J, Jacobs P, Martens J. Isomerization and hydrocracking of C_9 through C_{16} n-Alkanes on Pt/HZSM-5 zeolite. *Appl Catal*. 1983;8:123–141.
34. McVicker G, Daage M, Touvelle M, Hudson C, Klein D, Baird Jr. W. Selective ring opening of naphthenic molecules. *J Catal*. 2002;210:137–148.
35. Mouli KC, Sundaramurthy V, Dalai AK, Ring Z. Selective ring opening of decalin with Pt-Ir on Zr modified MCM-41. *Appl Catal, A*. 2007;321:17–26.
36. Cooper BH, Donnis BBL. Aromatic saturation of distillates: An overview. *Appl Catal, A*. 1996;137:203–223.
37. Vogel P. *Carbocation Chemistry*. Amsterdam: Elsevier; 1985.
38. Gnep S, Guisnet M. Aromatization of propane over gahmfi catalysts. reaction scheme, nature of the dehydrogenating species and mode of coke formation. *Catal Today*. 1996;31:275.
39. Al-Khattaf S, Atias JA, Jarosch K, de Lasa HI. Diffusion and catalytic cracking of 1,3,5 tri-iso-propyl-benzene in FCC catalysts. *Chem Eng Sci*. 2002;57:4909–4920.
40. Al-Khattaf S, de Lasa H. Diffusion and reactivity of gas oil in FCC catalysts. *Can J Chem Eng*. 2001;79:341–348.
41. Van Landeghem F, Nevicato D, Pitault I, Forissier M, Turlier P, Derouin C, Bernard JR. Fluid catalytic cracking: modelling of an industrial riser. *Appl Catal, A*. 1996;138:381–405.
42. Froment GF, Bischoff KB. *Chemical Reactor Analysis and Design*. 2nd ed. New York: Wiley; 1979.
43. Atias JA, Tonetto G, de Lasa H. Modeling fluid catalytic cracking in a novel crec riser simulator: adsorption parameters under reaction conditions. *Int J Chem React Eng*. 2003;1(A-50):1–25.
44. Ruthven DM, Kaul BK. Adsorption of aromatic hydrocarbons in NaX Zeolite. 1. Equilibrium. *Ind Eng Chem Res*. 1993;32:2047–2052.
45. Coleman TF, Li Y. An interior, trust region approach for nonlinear minimization subject to bounds. *SIAM J Optim*. 1996;6:418–445.

Manuscript received Oct. 9, 2008, and revision received Dec. 17, 2008.